Benguela Niños and Benguela Niñas in Forced Ocean Simulation From 1958 to 2015

Rodrigue Anicet Imbol Koungue, Mathieu Rouault, Serena Illig, Peter Brandt, Julien Jouanno

▶ **To cite this version:**

Rodrigue Anicet Imbol Koungue, Mathieu Rouault, Serena Illig, Peter Brandt, Julien Jouanno. Benguela Niños and Benguela Niñas in Forced Ocean Simulation From 1958 to 2015. Journal of Geophysical Research. Oceans, 2019, 124 (8), pp.5923-5951. 10.1029/2019JC015013 . ird-04559062

HAL Id: ird-04559062
https://ird.hal.science/ird-04559062v1

Submitted on 5 May 2024

HAL is a multi-disciplinary open access archive for the deposit and dissemination of scientific research documents, whether they are published or not. The documents may come from teaching and research institutions in France or abroad, or from public or private research centers.

L'archive ouverte pluridisciplinaire **HAL**, est destinée au dépôt et à la diffusion de documents scientifiques de niveau recherche, publiés ou non, émanant des établissements d'enseignement et de recherche français ou étrangers, des laboratoires publics ou privés.

Distributed under a Creative Commons Attribution 4.0 International License

Check for updates

JGR Oceans

RESEARCH ARTICLE
10.1029/2019JC015013

Benguela Niños and Benguela Niñas in Forced Ocean Simulation From 1958 to 2015

Rodrigue Anicet Imbol Koungue[1,2,3], Mathieu Rouault[2,3], Serena Illig[2,4], Peter Brandt[1,5], and Julien Jouanno[4]

[1]GEOMAR Helmholtz Centre for Ocean Research Kiel, Kiel, Germany, [2]Department of Oceanography, MARE Institute, University of Cape Town, Cape Town, South Africa, [3]Nansen-Tutu Centre for Marine Environmental Research, Department of Oceanography, University of Cape Town, Rondebosch, South Africa, [4]Laboratoire d'Etudes en Géophysique et Océanographie Spatiales (LEGOS), Université de Toulouse, CNES, CNRS, IRD, UPS, Toulouse, France, [5]Faculty of Mathematics and Natural Sciences, Christian-Albrechts-Universität zu Kiel, Kiel, Germany

Key Points:
- Over 1958–2015, we document the development of Benguela Niño and Niña events occurring along the southwestern African coast
- They are associated with coastally trapped waves dominantly forced by eastward propagating equatorial Kelvin waves of second baroclinic mode
- They are linked to large-scale wind stress forcing one to two months before they peak usually in March–April

Supporting Information:
- Supporting Information S1

Correspondence to:
R. A. Imbol Koungue,
rodrigueanicet@gmail.com

Citation:
Imbol Koungue, R. A., Rouault, M., Illig, S., Brandt, P., & Jouanno, J. (2019). Benguela Niños and Benguela Niñas in forced ocean simulation from 1958 to 2015. *Journal of Geophysical Research: Oceans*, *124*, 5923–5951. https://doi.org/10.1029/2019JC015013

Received 29 JAN 2019
Accepted 29 JUL 2019
Accepted article online 04 AUG 2019
Published online 19 AUG 2019

The copyright line for this article was changed on 30 DEC 2019 after original online publication.

Abstract A systematic study of Benguela Niño and Benguela Niña events during 1958 to 2015 including those that developed before the satellite era (1982) is carried out using an ocean general circulation model in combination with a linear equatorial model. Altogether, 21 strong warm and cold anomalous coastal events are identified among which 6 undocumented extreme coastal events are reported. Results suggest that most of these extreme coastal events including the newly identified ones are linked to remote equatorial forcing via mode 2 equatorial Kelvin waves. The latter propagates after approaching the African coast poleward as coastally trapped waves leading surface temperature anomalies along the Angola-Benguela current system by one month. One to two months before the peak of Benguela Niños or Niñas usually occurring in March–April, a large-scale wind stress forcing is observed with both local (variations of alongshore coastal wind stress) and remote forcing developing simultaneously. Results further suggest that surface temperature anomalies off Southern Angola and in the Angola-Benguela Front are associated with equatorial dynamics and meridional wind stress fluctuations off the southwestern African coast north of 15°S. Similar mechanisms are observed for Northern Namibia in combination with forcing by local meridional wind stress variations.

Plain Language Summary The Benguela upwelling system located in the southeastern Atlantic Ocean supports a large marine ecosystem due to upwelling conditions. Every few years, anomalous warm and cold coastal events occur in the southeastern Atlantic and are detrimental for Angola, Namibia, and South Africa, as they affect fisheries and rainfall like El Niño phenomenon in the Pacific. To study these coastal events from 1958 to 2015, we use the output from a tropical Atlantic simulation in combination with the solution of a simple linear equatorial model. We study the anomalous coastal events including the ones that occurred before the satellite era (before 1982) and examine the role of the local wind forcing and the remote forcing associated with equatorial variability. We describe so far undocumented extreme events occurring from 1958 to 2015. Results suggest that most of the extreme coastal warm and cold events are associated with the propagation of equatorial Kelvin waves along the equatorial waveguide which trigger poleward-propagating coastal trapped waves along the southwestern African coast. One to two months before the peak season (usually March–April) of the anomalous coastal events, a large-scale wind pattern is observed, encompassing both variations of alongshore coastal wind in the southeastern Atlantic and zonal wind along the equatorial Atlantic.

1. Introduction

The Benguela Upwelling Systems (BUS) is among the most productive marine ecosystems in the world ocean supporting important fisheries (Chavez & Messié, 2009) due to upwelling dynamics. Compared to the other Eastern Boundary Upwelling Systems, one of the main specific features of the BUS is that it is encircled by warm waters at its northern and southern boundaries: tropical water from the equatorial Atlantic in the north and warm water coming from the Agulhas Current in the south. The convergence zone between the warm equatorial waters and the cold upwelled waters from the BUS forms a well-defined meridional thermal front called Angola-Benguela Front (ABF; Shannon et al., 1987; Mohrholz et al., 2001; Veitch et al., 2006). Veitch et al. (2006) quantified a meridional sea surface temperature (SST) gradient of 1 °C per 34 km (or 3

©2019. The Authors.
This is an open access article under the terms of the Creative Commons Attribution License, which permits use, distribution and reproduction in any medium, provided the original work is properly cited.

°C per 100 km) across the ABF in austral summer, whereas ~4 °C per 100 km was estimated by Colberg and Reason (2006) in the middle of the ABF. On average, the ABF is located at around ~17°S (Veitch et al., 2006).

The BUS experiences an important variability at a wide range of frequencies and in particular at interannual time scales. Every few years, the BUS is anomalously warm. These extreme warm events are called Benguela Niños (Shannon et al., 1986; Florenchie et al., 2004; Rouault et al., 2007; Ostrowski et al., 2009; Imbol Koungue et al., 2017; Rouault et al., 2018). The inverse of a Benguela Niño is called Benguela Niña (Florenchie et al., 2004; Imbol Koungue et al., 2017). These events typically manifest along the coast of Angola and Namibia in the southeastern Atlantic Ocean and tend to reach their maximum in late austral summer mainly during March–April (Florenchie et al., 2003, 2004; Lübbecke et al., 2010; Rouault et al., 2007). During a Benguela Niño event, SST can reach up to 4 °C above the seasonal average (Rouault et al., 2018). Extreme coastal events (Benguela Niño or Niña) can last from few months to half a year or more (Florenchie et al., 2004; Rouault, 2012; Rouault et al., 2003). They impact on the regional climate and rainfall (Hansingo & Reason, 2009; Rouault et al., 2003, 2009), responsible for drought or flooding in the neighboring countries. They also affect the ecosystem and the productivity through a change in the upwelling intensity that modulates the biogeochemical properties and fish habitat (Blamey et al., 2015; Boyer et al., 2001; Ostrowski et al., 2009).

From previous studies, two principal forcing mechanisms responsible for the interannual variability of SST in the Angola-Benguela current system are still under debate, that is, local atmospheric forcing and the connection with the equatorial variability. On the one hand, Richter et al. (2010) using observations along with a coupled ocean–atmosphere simulations showed that local alongshore wind modulations related to the magnitude and location of South Atlantic Anticyclone (SAA) are responsible for the coastal SST variability in the southeastern Atlantic Ocean. Also, Polo et al. (2008) suggested that SST anomalies (SSTA) off Angola are generated by upwelling anomalies caused by local winds. For the warm event in early 2016, Lübbecke et al. (2019) further discussed other local processes contributing to the development of this specific warm event including reduced cooling by atmospheric heat fluxes, reduced mixing associated with enhanced freshwater input into the surface ocean, and anomalous poleward advection of warm anomalies in the surface layer by reduced winds. On the other hand, past studies indicated that remote forcing is the main triggering process that explains the occurrence of Benguela Niño and Niña events. Remote forcing is associated with eastward propagation of equatorial Kelvin waves along the Atlantic equator triggered by a sudden change in the easterlies in the western or central equatorial Atlantic. Note that Bachèlery et al. (2016) mentioned in their modeling study that equatorial Kelvin waves could also be forced in the eastern equatorial Atlantic (Gulf of Guinea) by zonal wind stress variations. Equatorial Kelvin waves propagate up to the African coast where part of their energy is reflected westward as equatorial Rossby waves while a substantial amount is transmitted poleward as coastal trapped waves (CTWs; Clarke, 1983) influencing the near-coastal temperature variability downstream along the southwestern coast of Africa (Bachèlery et al., 2016). This wave dynamics could be at the origin of anomalously warm and cold events in the Angola-Benguela current system (Florenchie et al., 2003, 2004; Rouault et al., 2007, 2018; Ostrowski et al., 2009; Lübbecke et al., 2010; Bachèlery et al., 2016; Imbol Koungue et al., 2017). According to Bachèlery et al. (2016), the efficiency by which CTWs could trigger temperature anomalies through vertical advection and mixing is controlled by the vertical stratification of the water column along the southwestern African coast. At the seasonal scale, Tchipalanga et al. (2018) showed that off Angola, the upper-ocean stratification increases in austral summer and decreases in austral winter, which makes the impact of CTWs more efficient during austral summer. CTWs have also a significant influence on the eastern boundary circulation. According to the modeling study of Bachèlery et al. (2016), during the developing phase of the downwelling event, the corresponding downwelling CTW is associated with a poleward velocity anomaly, which is strongest near the coast below 40-m depth. It is associated with an anomalous decrease of the upward current leading to a substantial reduction of the seasonal upwelling near the coast. Conversely, during the developing phase of an upwelling event, the upwelling CTW is associated with increased equatorward and upward currents in the upper 200 m resulting in enhanced coastal upwelling of cold nutrient-rich waters along the coast and the appearance of near-coastal cold temperature anomalies at the sea surface. The superposition of CTWs and the local currents could strengthen the poleward or equatorward transport of warm equatorial or cold upwelled waters across the ABF, which is a key element in the development of Benguela Niños or Niñas (Rouault, 2012).

21699291, 2019, 8, Downloaded from https://agupubs.onlinelibrary.wiley.com/doi/10.1029/2019JC015013 by Cochrane France, Wiley Online Library on [04/05/2024]. See the Terms and Conditions (https://onlinelibrary.wiley.com/terms-and-conditions) on Wiley Online Library for rules of use; OA articles are governed by the applicable Creative Commons License

21699291, 2019, 8, Downloaded from https://agupubs.onlinelibrary.wiley.com/doi/10.1029/2019JC015013 by Cochrane France, Wiley Online Library on [04/05/2024]. See the Terms and Conditions (https://onlinelibrary.wiley.com/terms-and-conditions) on Wiley Online Library for rules of use; OA articles are governed by the applicable Creative Commons License

Recently, Imbol Koungue et al. (2017) combined real-time buoy measurements from the Prediction and Research Moored Array in the Tropical Atlantic (PIRATA), altimetric sea surface height (SSH), and an equatorial Ocean Linear Model (OLM) in order to identify propagation of SSH anomalies (SSHA) along the equator and define an equatorial oceanic index of interannual equatorial Kelvin wave (IEKW) amplitude using the OLM. From 1998 to 2012, they succeeded to link this IEKW proxy to the coastal variability off Angola and Namibia in order to forecast Benguela Niños or Niñas which are of great socioeconomic importance for the countries of Southern Africa. However, little is known concerning the Benguela Niños and Niñas that occurred before the satellite era, that is, before 1982.

The aim of this study is to document potential processes that are at work during the onset and the development of the coastal events including the events that occurred before the satellite era. Due to the good agreement between PIRATA dynamic height and the OLM SSHA in the monitoring of the IEKW from 1998 to 2012 (cf. Imbol Koungue et al., 2017, Table 1), OLM outputs from 1958 to 2015 were derived. Our methodology is then based on the combination of analysis of an Ocean General Circulation Model (OGCM) output of the tropical Atlantic and of the OLM output from 1958 to 2015 in order to study the anomalous coastal events developing before 1982. The OGCM also allows the calculation of the net subsurface ocean transport across the ABF, which is a key factor during the development of Benguela Niños (Rouault, 2012). This study is structured as follows: section 2 gives an overview of the different products used in this study, presents the methodology, and provides a validation of the model outputs at seasonal and interannual time scales. Section 3 is dedicated to the results. First, we present the identification and classification of all the anomalous SST coastal events in the Angola-Benguela upwelling system from 1958 to 2015. Second, we discuss the forcing mechanisms by quantifying the remote equatorial forcing, the role of large-scale wind stress, and the potential role of the coastal wind stress. Third, newly identified extreme warm and cold events are described. Section 3.3.4 provides a discussion of the results, conclusions, and perspectives to this study.

2. Data, Model, Methodology, and Model Validation

Observational data sets and reanalyses are used to evaluate the OGCM performances along the equatorial Atlantic and the Angola-Benguela upwelling system in surface and subsurface from 1958 to 2015.

2.1. Observational Data

2.1.1. PIRATA Moorings

PIRATA buoys have been deployed in the tropical Atlantic since September 1997 (Bourlès et al., 2008; Servain et al., 1998). PIRATA program is composed of an array of moorings in the Atlantic Ocean. PIRATA moorings record and sample the water column with five temperature/conductivity sensors deployed at depths of 1, 10, 20, 40, and 120 m; five temperature sensors positioned at depths of 60, 80, 100, 140, and 180 m; and two temperature/pressure sensors positioned at 300 and 500 m along the equatorial Atlantic. Data display, download, climatology estimations, and additional information are available on the dedicated website (http://www.pmel.noaa.gov/tao/disdel/).

Monthly dynamic height from three PIRATA's buoys located along the equator at 23°W, 10°W, and 0°E is used in this study from 1998 to 2015. It is worth mentioning that PIRATA records contain gaps at various locations due to vandalism or data failure. Refer to Imbol Koungue et al. (2017) for systematic quantification of these gaps over the 1998–2012 period.

2.1.2. Optimum Interpolation Sea Surface Temperature Version 2

We use the monthly Optimum Interpolation SST version 2 (OI-SST v2; Reynolds et al., 2002) available at 1° × 1° horizontal resolution since 1982. Data can be downloaded from the NOAA website (https://www.esrl.noaa.gov/psd/data/gridded/). This data set is derived from daily merged in situ and remote sensed data.

2.1.3. World Ocean Atlas 2013 Version 2

The World Ocean Atlas 2013 version 2 (WOA13v2) allows evaluating the OGCM skills in the tropical Atlantic in representing the mean vertical structure of temperature along the Atlantic equatorial waveguide and at 23°S in the southeastern Atlantic Ocean. WOA13v2 monthly climatology was chosen from 1955 until 2012 (an average of six decadal means) in the upper 250 m. WOA13v2 monthly climatology is a gridded product derived from in situ measurements (for example, ship-deployed Conductivity-Temperature-Depth, Expendable Bathythermographs, gliders, and moored and drifting buoys), interpolated and produced at a 0.25° × 0.25° resolution. It contains 102 vertical levels from the surface (0 m) to 5,500 m (Locarnini et al.,

21699291, 2019, 8, Downloaded from https://agupubs.onlinelibrary.wiley.com/doi/10.1029/2019JC015013 by Cochrane France, Wiley Online Library on [04/05/2024]. See the Terms and Conditions (https://onlinelibrary.wiley.com/terms-and-conditions) on Wiley Online Library for rules of use; OA articles are governed by the applicable Creative Commons License

2013). The data are processed by NOAA and archived at the National Oceanographic Data Center. The data are available on the website http://www.nodc.noaa.gov/OC5/woa13/.

2.1.4. Altimetry

The reference altimetric SSH gridded product, distributed by the Archiving, Validation, and Interpretation of Satellite Oceanographic Data (AVISO), merges data from TOPEX/Poseidon and Jason-1/2/3 altimeters. The data are compared to the tropical Atlantic OGCM and the linear model for the purpose of model validation (cf. section 2.4). Data are distributed by Collected Localisation Satellites (CLS) on a weekly temporal resolution available on a 1/4° horizontal resolution grid. Refer to Le Traon et al. (1998) and Ducet et al. (2000) for more details on data and gridding procedures.

2.2. Model Configurations

2.2.1. Tropical Atlantic OGCM Simulation

The OGCM numerical model used in this study is the oceanic component of the Nucleus for European Modelling of the Ocean program (NEMO3.6) (Madec, 2014). It solves the Navier-Stokes primitive equations under spherical coordinates discretized on a C-grid and fixed vertical levels (z coordinate). The parameterization and the physical parameters are similar to those of Hernandez et al. (2016, 2017). The regional grid has 0.25° horizontal resolution and extends from 98.50°W to 19.80°E, and from 34.05°S to 33.73°N. There are 75 vertical levels, with 12 levels within the first 20 m and 24 levels within the first 100 m. The momentum advection scheme is the third-order upstream biased scheme with no explicit diffusion. Tracers are advected with a total variance dissipation scheme, and a Laplacian isopycnal diffusion is applied with a diffusion coefficient of 300 m^2/s. The model time step is 1,200 s. The vertical diffusion coefficient is estimated using the generic length-scale scheme with a k-epsilon turbulent closure (Umlauf & Burchard, 2003). More details can be found in Reffray et al. (2015) and Maraldi et al. (2013). A seasonal climatology built from daily outputs of the MERCATOR global reanalysis GLORYS2V3 for the period 1993–2012 has been used to force the model at its two open lateral boundaries. The atmospheric fluxes of momentum, heat, and freshwater at the surface are given by bulk formulae (Large & Yeager, 2009) using 3-hr fields of wind speed, atmospheric temperature, and humidity, and daily fields of longwave, shortwave radiation, and precipitation from the DRAKKAR Forcing Set version 5.2 (DFS5.2; Dussin et al., 2016). DFS5.2 is actually a corrected forcing for DRAKKAR simulation using ERA-Interim atmospheric reanalysis (Dee et al., 2011). The shortwave radiation forcing is modulated online by an analytical diurnal cycle. The penetration of the solar radiation (decomposed in three wavebands; Red-Green-Blue) is modulated by a spatially and seasonally varying estimate of upper ocean chlorophyll concentrations using the empirical parameterization from Morel et al. (1989). Here we use a seasonal climatology of surface chlorophyll concentrations to force the model that has been constructed from the GlobColour monthly merged MODIS/VIIRSN gridded product (Maritorena et al., 2010). Details on the methodology are given in Hernandez et al. (2017). Taking into account the chlorophyll concentrations leads to differential heating of the upper ocean that ultimately improves the representation of SST in the Benguela upwelling system (Hernandez et al., 2017). There is no explicit restoring of the SST, but the specification of atmospheric conditions (air temperature, humidity, and wind speed) when forcing the ocean model with the bulk formulae in the simulation acts to restore the SST toward prescribed air temperature. This may participate to counterbalance model biases in reproducing the Benguela upwelling variability. There is also no restoring toward observed or climatological sea surface salinity (Hernandez et al., 2016). A monthly climatological runoff based on the data set of Dai and Trenberth (2002) is prescribed near the river mouths as a surface freshwater flux with increased vertical mixing in the upper 10 m. The OGCM has been integrated over the period 1958–2015 (Hernandez et al., 2017) and monthly averages were analyzed in this work.

2.2.2. OLM

A simulation was carried out with the equatorial Atlantic OLM developed by Illig et al. (2004). The latter was used in Rouault et al. (2007, 2018), Imbol Koungue et al. (2017), and Illig and Bachèlery (2019) to examine the mechanisms associated with equatorial Kelvin wave propagations and their connection with the coastal variability. It is also used here to interpret the OGCM outputs in terms of equatorial wave propagations. The simulation of the eastward and westward propagations of equatorial Kelvin and Rossby waves, respectively, in the equatorial band is performed within a domain extending from 50°W to 10°E and from about 29°S to 29°N, with a horizontal resolution of 2° in longitude and 0.25° in latitude. It includes six baroclinic modes with phase speed, wind stress projection coefficient, and friction estimated according to Illig et al. (2004).

21699291, 2019, 8, Downloaded from https://agupubs.onlinelibrary.wiley.com/doi/10.1029/2019JC015013 by Cochrane France, Wiley Online Library on [04/05/2024]. See the Terms and Conditions (https://onlinelibrary.wiley.com/terms-and-conditions) on Wiley Online Library for rules of use; OA articles are governed by the applicable Creative Commons License

For consistency with the OGCM simulation, the OLM is forced by two-day DFS5.2 detrended interannual wind stress anomalies (cf. section 2.3.1) estimated over the 1958–2015 period.

2.3. Methodology

2.3.1. Interannual Monthly Anomalies

First, the high-frequency variability (mainly submonthly component) is filtered out by averaging all data into monthly data and using monthly averaged model outputs in this study. To compute the interannual monthly anomalies, monthly climatology (estimated over the period of interest) is removed from the initial monthly time series. The obtained time series includes also intraseasonal variability with periods smaller than the seasonal cycle and larger than two months. The filtering of the intraseasonal variability will be explained in section 2.3.5. Since interannual variability is the time scale of interest and a linear trend or decadal variability in SST is observed over the Angola-Benguela upwelling system, we removed the linear trend before computing the anomalies. To do so, the linear least squares regression fit is estimated and is removed from the original time series. A similar methodology was used in Imbol Koungue et al. (2017).

2.3.2. Normalization of Anomalies

Two different methods are used for the normalization of the monthly anomalies time series. Method 1 is the normalization by the monthly standard deviation (STD) when each monthly interannual monthly anomaly is divided by the standard deviation of that month as done in Rouault (2012) and Imbol Koungue et al. (2017). In method 2, monthly interannual anomalies are normalized by the STD of the entire time series. This method is also called standard scores (z-scores). It is used when it is not possible to implement method 1. For example, gaps occurring in a data set such as PIRATA records prevent a good estimation of the seasonal phasing of the interannual variability.

2.3.3. Taylor Diagrams

Taylor diagrams (Taylor, 2001) are used to compare the OGCM outputs to available observation data sets such as PIRATA, WOA13v2, and AVISO. Taylor diagram provides the degree of correspondence between observed and simulated time series in terms of four statistics: the Pearson correlation coefficient, the root-mean-square difference (RMSD), and the STD of observation and simulation. The relationship between these four statistics is similar to the triangular geometric relationship given by the law of cosines (see Taylor (2001) for more details). The Taylor diagram is then a summary polar plot in which correlation coefficients between observations and simulation time series are given by the azimuthal angle. The best agreement between model outputs and observations is observed when the RMSD is close to zero and the correlation is close to 1. The Taylor diagrams used in this study are customized such that the radial distance from the origin is proportional to the standard deviation of a pattern normalized by the standard deviation of the observations and the green dashed circular lines measure the distance from the reference point (Black point, Ref) that measures the RMSD (e.g., Figure 1c).

2.3.4. Description of the Coastal Domains of Interest

The interannual SST coastal variability along the western coast of Africa is studied within three key domains as defined in Rouault et al. (2018) which are illustrated in Figure 2d: (1) the Southern Angola domain (10°S–15°S; 1°-width coastal fringe), a low wind speed tropical warm water region affected by the Angola Current (Kopte et al., 2017; Tchipalanga et al., 2018) and CTWs; (2) the ABF domain (15°S–19°S; 1°-width coastal fringe), which is a transition region between the warm tropical water and cold upwelled water separated by the ABF in its middle; and (3) the Northern Namibia domain (19°S–24°S; 1°-width coastal fringe), a wind-driven upwelling region with cold upwelled waters best characterized as Northern Benguela Upwelling System (NBUS).

2.3.5. Criteria for Anomalous Coastal Events

First, we want to highlight the fact that the OGCM temperature at 10 m (hereafter T10) is used instead of OGCM SST in this study. The reason is that the OGCM SST could be impacted by turbulent heat fluxes and related net heat flux forcing at the surface resulting from prescribed atmospheric fields. However, there is no significant difference between the two simulated OGCM temperature at the surface and at 10-m depth (not shown), because both levels are found within the model mixed layer. To comment on the coastal T10 variability along the western coast of Africa, three coastal domains of interest are taken within the 1°-width coastal band. Their geographical positions are described in section 2.3.4 and depicted in Figure 2d. Criteria are defined to identify anomalous coastal events which are divided into two categories, namely, extreme and moderate coastal events. As in Imbol Koungue et al. (2017), an extreme warm or cold coastal event occurs

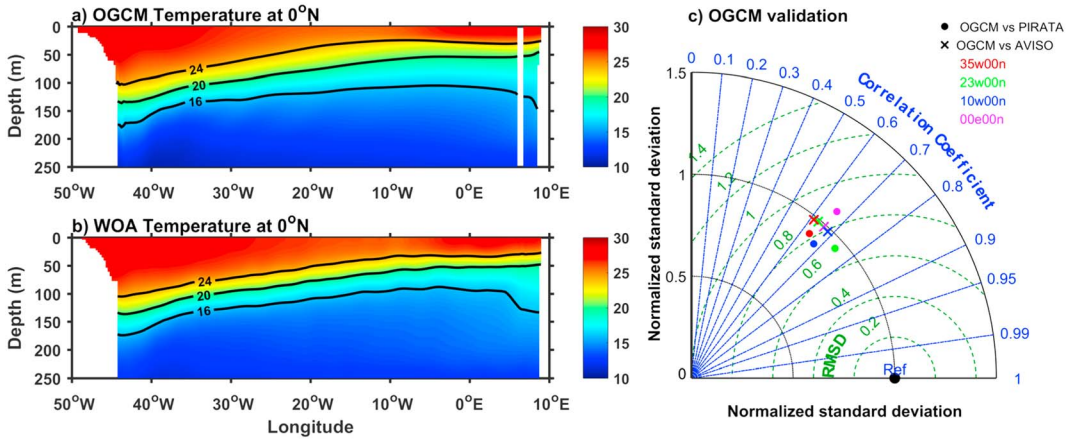

Figure 1. (a) Longitude-depth section of the OGCM mean (1958–2015) temperature (°C) along the equator (0°N). Thick black lines highlight the position of the 16 °C, 20 °C, and 24 °C isotherms. (b) Same as in (a) but for WOA13v2 (1955–2012). (c) Taylor diagram comparing OGCM detrended normalized interannual anomalies of OGCM SSH to PIRATA dynamic height estimations (points) and AVISO SSH data (stars). Comparisons are performed along the equatorial Atlantic at (35°W, 23°W, 10°W, 0°E; 0°N) over the period 1998–2015.

when detrended normalized T10 anomalies (hereafter DNT10A) exceed the threshold of ±1 STD for at least three consecutive months in at least two domains. This helps filtering out most of the intraseasonal variability (shortest periods). Moderate warm or cold events are identified when DNT10A exceed the threshold of ±1 STD for two consecutive months in at least two domains.

2.3.6. Composite and Bootstrap

In this study, both composites of detrended anomalies of T10 (hereafter DT10A) and wind stress are estimated over four extreme coastal warm (1976/1977, 1984, 1995, and 2001) and four extreme cold (1981/1982, 1985, 1991/1992, and 1996/1997) events which peak in March–April (Florenchie et al., 2003, 2004; Lübbecke et al., 2010; Lübbecke et al., 2019; Rouault, 2012; Rouault et al., 2007).

The bootstrap method is used to test the statistical significance of composite maps. This method allows calculating the statistically significant areas in composite maps of DT10A. The bootstrap technique is a nonparametric test which is independent of the distribution of the data. The bootstrap method was introduced by Efron, 1977 (Diaconis & Efron, 1983). The basic idea when performing the bootstrap is to construct a large collection of artificial data groups having the same size as the composite group. For this study, the target group corresponds to the occurrences of four anomalous extreme warm or cold events leading to a composite map for each category of events. The 10,000 artificial data groups are randomly generated from the initial data set. Note that there are two different ways to perform the bootstrap test: with or without replacement (Grotjahn & Faure, 2008). For this study, the bootstrap testing without replacement is chosen meaning that the months among each randomly picked group are all different. In this case, the initial monthly data set is resampled 10,000 times to form 10,000 artificial averages. These 10,000 artificial averages are then sorted in ascending order. Therefore, each grid point of the composite map will be statistically significant at 90% if its value belongs to the upper 5% or lower 5% outlier of the artificial group distribution.

2.4. OGCM Validation

This section is dedicated to the validation of the OGCM tropical Atlantic simulation. First, a comparison between the equatorial mean structure of temperature from the tropical Atlantic simulation (OGCM) from 1958 to 2015 and from WOA13v2 (1955–2012) in the upper 250 m from 50°W to 10°E is performed (cf. Figures 1a and 1b). The OGCM thermocline (identified by the depth of the isotherm 20 °C; Z20) is well positioned along the equatorial waveguide, deeper in the western equatorial Atlantic, and shallower in the Gulf of Guinea with warm waters in the upper layers and cold waters below the thermocline (Figure 1a).

On average along the equator, the simulated thermocline depth (Z20) is ~1.32 m deeper than the observed one (not shown). However, Figure 1b shows that the thickness of the equatorial thermocline delimited by the thickness of the layer between the 16 °C and 24 °C isotherms is too diffuse in the simulation (Figure 1a) along the equatorial Atlantic with weaker (−21%) vertical gradients than WOA13v2. To

21699291, 2019, 8, Downloaded from https://agupubs.onlinelibrary.wiley.com/doi/10.1029/2019JC015013 by Cochrane France, Wiley Online Library on [04/05/2024]. See the Terms and Conditions (https://onlinelibrary.wiley.com/terms-and-conditions) on Wiley Online Library for rules of use; OA articles are governed by the applicable Creative Commons License

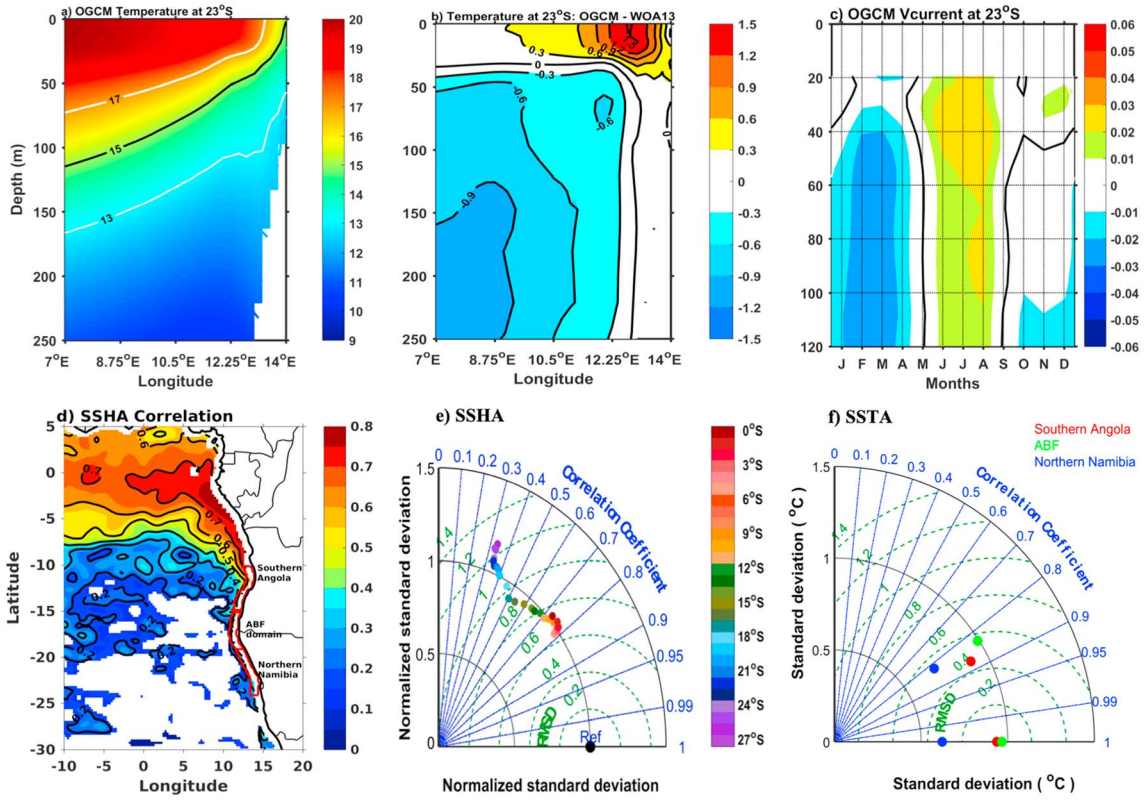

Figure 2. (a) OGCM mean (1958–2015) vertical temperature (°C) cross-shore section at 23°S as a function of longitude and depth (m). The black (white) lines represent the mean position of the 15 °C (17 °C and 13 °C) isotherms. (b) Difference between OGCM and observed (WOA13v2) mean vertical temperature (°C) section at 23°S, with contours every 0.3 °C. (c) OGCM vertical profile of climatological meridional current velocities (m/s) at (14°E, 23°S) to be compared to the ADCP climatology presented in Junker et al. (2017), their Figure 6a). The monthly mean climatology is computed over the 2003–2015 period. Positive (negative) current velocity values mean northward (poleward) directed currents. (d) Correlation map between observed monthly detrended interannual AVISO SSHA and OGCM SSHA over the 1993–2015 period in the southeastern Atlantic Ocean. The white area depicts correlations nonstatistically significant at 95% (Sciremammano, 1979). Contours are every 0.1. Red contours highlight the positions of the three coastal domains of interest (see section 2.3.4). (e) Taylor diagram illustrating the OGCM skills in representing the altimetric detrended normalized SSHA along the southwestern African coast (averaged within the 1°-width coastal fringe) over 1993–2015. Colors indicate the latitude. To subtract the mesoscale variability, time series are preliminarily smoothed using a 5°-width latitudinal running average filter. (f) Taylor diagram comparing the OGCM and OI-SST detrended SSTA averaged within the three coastal (averaged within the 1°-width coastal fringe) domains of interest (section 2.3.4), namely, Southern Angola (10°–15°S), ABF domain (15°S–19°S), and Northern Namibia (19°S–24°S) over the 1982–2015 period. Colored dots on the *x* axis represent the observations (OI-SST) in each domain.

estimate the realism of the OGCM in simulating the equatorial interannual variability, Figure 1c presents a Taylor diagram comparing model detrended normalized (using standard scores; cf. section 2.3.2) anomalies of SSH and PIRATA dynamic height, along the equatorial Atlantic (0°N) at the 35°W, 23°W, 10°W, and 0°E. Results show that the OGCM agrees best with PIRATA observations at (23°W, 0°N) and (10°W, 0°N). At these two locations, the RMSD is lower than 0.8 cm and correlation coefficients equal to 0.74 and 0.67, respectively. The magnitude of the OGCM interannual activity is of the same order as AVISO SSHA, as indicated by the normalized STD close to 1 at each PIRATA mooring location. The correlation coefficient ranges between 0.6 and 0.7, being statistically significant at 95% (Sciremammano, 1979). In conclusion, the mean state (temperature) and the interannual variability (SSH) simulated by the OGCM are quite realistic along the equatorial Atlantic. This means that the interannual OGCM shows good skills in representing the equatorial dynamics.

Along the southwestern African coast, the mean simulated cross-shore vertical structure of the temperature in the upper 250 m at 23°S from 7°E to 14°E is presented in Figure 2a. The simulation represents quite well the signature of the coastal upwelling off the Namibian coast with the 15 °C isotherm tilted upward toward the coast and almost outcropping at the surface near the coast (Figure 2a). Figure 2b shows that the simulation is warmer than the observations above 30-m depth and cooler below. Largest differences of 1.4 °C to 2 °C appear

21699291, 2019, 8, Downloaded from https://agupubs.onlinelibrary.wiley.com/doi/10.1029/2019JC015013 by Cochrane France, Wiley Online Library on [04/05/2024]. See the Terms and Conditions (https://onlinelibrary.wiley.com/terms-and-conditions) on Wiley Online Library for rules of use; OA articles are governed by the applicable Creative Commons License

21699291, 2019, 8, Downloaded from https://agupubs.onlinelibrary.wiley.com/doi/10.1029/2019JC015013 by Cochrane France, Wiley Online Library on [04/05/2024]. See the Terms and Conditions (https://onlinelibrary.wiley.com/terms-and-conditions) on Wiley Online Library for rules of use; OA articles are governed by the applicable Creative Commons License

close to the coast in the upper 30 m within around 400-km-wide coastal band. Differences are associated with warm biases often encountered in simulations of the Angola-Benguela current system. Similar results were obtained in the study by Bachèlery et al. (2016) in the upper layer at the same location.

Because of the importance of meridional velocities and corresponding water mass transfer across the ABF for the development of the Benguela Niños (Rouault, 2012), a validation of the meridional current velocities is also performed. Note that it was not possible to validate the OGCM meridional current velocities at interannual time scales due to the scarcity of ocean current observations. The validation is done instead for the mean seasonal cycle using moored ADCP data (Junker et al., 2017) taken at 23°S on the Namibian shelf at a water depth of 130 m during the period from 2003 to 2015 with some data gaps in between. Figure 2c shows the seasonal cycle of the vertical section of meridional current velocities from the OGCM taken at (14°E, 23°S) which has to be compared with the corresponding moored observations presented in Figure 7a in the study of Junker et al. (2017). There is a good representation of the seasonal cycle of meridional currents between the OGCM and the ADCP currents from Junker et al. (2017). Northward currents (positive values of meridional current velocities) are observed between May and September throughout the water column. Conversely, from October to April, the alongshore currents are mostly directed poleward (negative values of meridional current velocities). OGCM shows a weak equatorward flow (~0.01 cm/s) in the upper 45 m between October and December which was also observed by Junker et al. (2017), but in the upper 16 m. The relatively good agreement encourages us to use the OGCM to calculate meridional transport anomalies across the ABF.

Over the southeastern Atlantic Ocean, a correlation map between monthly interannual detrended anomalies of SSH using AVISO and the OGCM SSHA is estimated (Figure 2d) from 1993 to 2015. There is a good agreement between the OGCM and AVISO SSHA statistically significant at 95% (Sciremammano, 1979), along the equatorial waveguide with correlation larger than 0.7 from 0°E toward the West African coast. The zone of significant correlation expands poleward and is trapped to the African coast. A decrease in the southward direction up to around 25°S is observed close to the African coast. This suggests a dynamical connection between the equatorial domain and the coastal domain southward up to ~25°S which seems to be the limit where the signature of the CTWs is observable (Bachèlery et al., 2016). Offshore, the lack of significant correlation represented in white in Figure 2d highlights a mismatch between the OGCM and AVISO SSHA (non-statistically significant correlation at 95%). This area corresponds to the area of high mesoscale activity (presence of eddies) representing a stochastic process that results in low correlations. A Taylor diagram summarizes the comparison between OGCM and AVISO SSHA along the southwestern African coast within a 1-degree coastal band and for various 5°-width latitudinal bands, centered at each point between 0°S and 27°S over the 1993–2015 period. Latitudes are shown by the color of points according to the color bar in Figure 2e. As observed in Figure 2e, the correlation decreases, and the RMSD increases in a southward direction. This means that the disagreement between the model and the observations is much pronounced in the south. In the area between 0°S and 11°S, the simulated variability agrees well with the AVISO SSH because the amplitude or energy in the OGCM seems to be correct or comparable with the observed one (normalized standard deviation close to 1). Also, maximum correlation coefficients ranging between 0.7 and 0.8 are obtained between 0°S and 11°S. Figure 2f shows a Taylor diagram comparing detrended SSTA from OI-SST and OGCM averaged in the three coastal domains of interest (see section 2.3.4), namely, Southern Angola (red dot), the ABF (green dot), and Northern Namibia (blue dot). The correlation coefficient ranges between 0.8 and 0.9 for the three coastal domains of interest. The correlation slightly decreases in poleward direction. However, the RMSD is larger in the ABF domain compared to the other two domains. This could be due to the warm bias in the Angola-Benguela upwelling system present in the simulation.

In conclusion, the mean state simulated by the OGCM is quite realistic along the southeastern Atlantic Ocean (temperature and alongshore currents). Furthermore, the OGCM (SSH and SST) shows good skills in representing the interannual oceanic dynamics in the three coastal domains of interest of this study. The OGCM will thus provide a useful insight into the surface and subsurface processes associated with Benguela Niños and Niñas before the satellite era (before 1982).

Also, the OLM used in this study has been validated in Illig et al. (2004) over the period 1992–2000. It showed good skill in reproducing equatorial Atlantic dynamics. In this paper, the OLM outputs are used over a longer period and validated over the period 1993–2015. As expected, OLM SSHA and AVISO SSHA agree well in the equatorial waveguide along which the Kelvin and Rossby waves are propagating.

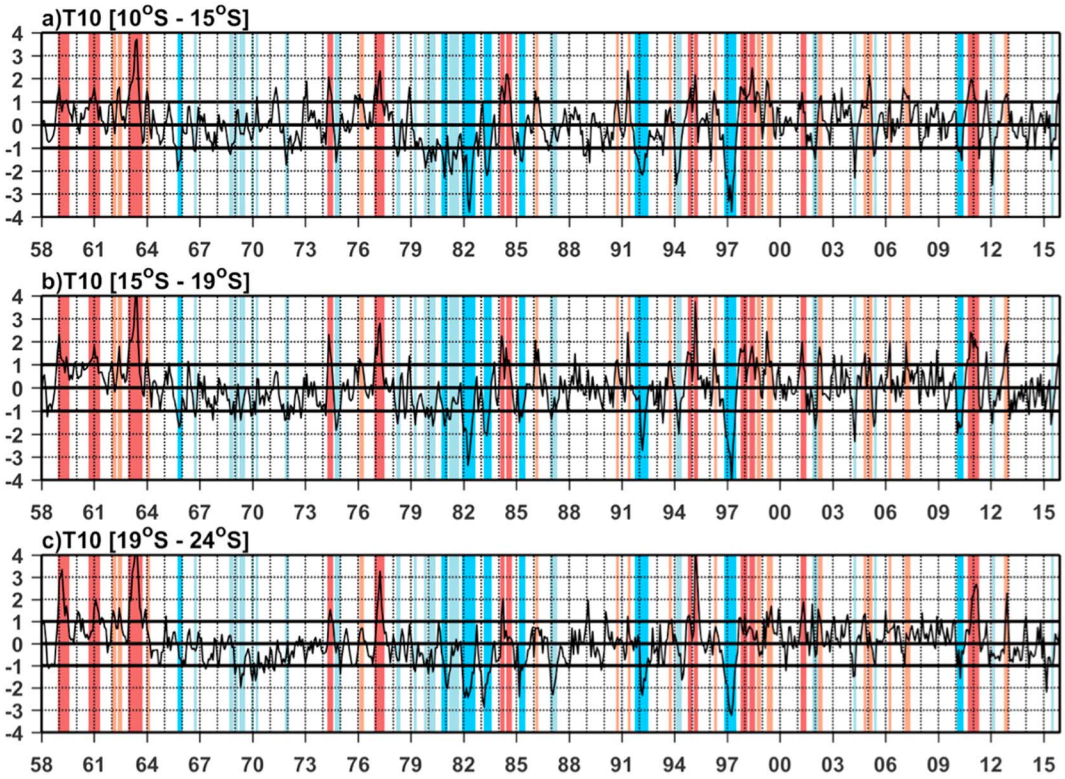

Figure 3. Monthly detrended normalized (by monthly STD) anomalies of coastal (averaged within the 1°-width coastal band) T10 (unitless) averaged along (a) Southern Angola (10°S–15°S), (b) ABF domain (15°S–19°S), and (c) Northern Namibia (19°S–24°S). Thick black horizontal lines emphasize our threshold (±1 standard deviation (STD)) used to detect extreme and moderate coastal T10 events. Red (blue) and light red (light blue) rectangles highlight extreme warm (cold) and moderate warm (cold) coastal events, respectively, along the Angolan-Namibian coastlines.

For instance, statistically significant correlations between monthly detrended SSHA from observation and OLM of 0.5, 0.56, and 0.63 (statistically significant at 95%; Sciremammano, 1979) are observed along the equatorial Atlantic between the AVISO SSHA and OLM SSHA at 23°W, 10°W, and 0°E, respectively.

3. Results

3.1. Identification and Classification of Anomalous Coastal Events

Figure 3 depicts the DNT10A (using method 1; cf. section 2.3.2) in the Angola-Benguela upwelling system averaged in the three coastal domains of interest (Southern Angola, ABF domain, and Northern Namibia) defined in section 2.3.4. Based on the criteria above defined (cf. section 2.3.5), 61 anomalous coastal events are identified and represented with colored rectangles in Figure 3. These anomalous coastal events are classified into 21 extreme coastal events (13 extreme warm and 8 extreme cold events) and 40 moderate coastal events (19 moderate warm and 21 moderate cold). In the supporting information, details in terms of duration and domains of occurrences are summarized (Tables S1 and S2 in the supporting information) and references to extreme events are given (Table S1 in the supporting information). The number of warm events (32) is superior to the number of cold events (29) which is consistent with the equatorial T10 signal which is positively skewed, with stronger warm events and weaker but longer-lasting cold events. For instance, the skewness of DT10A in the ABF domain (Figure 3a) is 0.1 and in Northern Namibia (Figure 3c) is 0.5. Previous studies identified some of these warm and cold events in the southeastern Atlantic Ocean. Stander and De Decker (1969), Shannon (1985), Hisard et al. (1986), Shannon et al. (1986), and Walker (1987) have identified early Benguela Niño events in 1963 and 1984.

Later events have been documented in the literature as well (Gammelsrød et al., 1998; Binet et al., 2001; Mohrholz et al., 2001; Hardman-Mountford et al., 2003; Florenchie et al., 2004; Reason et al., 2006; Rouault et al., 2007; Ostrowski et al., 2009; Lübbecke et al., 2010; Rouault, 2012; Imbol Koungue et al., 2017; Rouault et al., 2018). Note that the first to describe the 1995 warm event was Gammelsrød et al.

21699291, 2019, 8, Downloaded from https://agupubs.onlinelibrary.wiley.com/doi/10.1029/2019JC015013 by Cochrane France, Wiley Online Library on [04/05/2024]. See the Terms and Conditions (https://onlinelibrary.wiley.com/terms-and-conditions) on Wiley Online Library for rules of use; OA articles are governed by the applicable Creative Commons License

21699291, 2019, 8, Downloaded from https://agupubs.onlinelibrary.wiley.com/doi/10.1029/2019JC015013 by Cochrane France, Wiley Online Library on [04/05/2024]. See the Terms and Conditions (https://onlinelibrary.wiley.com/terms-and-conditions) on Wiley Online Library for rules of use; OA articles are governed by the applicable Creative Commons License

(1998) and the first study to detail the 1999 warm event was by Mohrholz et al. (2001). Our analysis allows to depict six new extreme coastal events (five of them occurring before the satellite era) which are not described in the previous studies, namely, the extreme warm events 1958/1959 (December–July), 1960/1961 (September–April), and 1974 (April–July). Similarly, undocumented extreme cold events are identified in 1965 (September–December), 1980/1981 (October–April), and 1985 (March–June). These extreme coastal events will be further described in section 3.2. Most of these extreme warm and cold events occurred in the three coastal domains of interest excluding the extreme cold event in 1965 (September–December) which developed only in the Southern Angola and ABF domains. There is a long cooling period from 1980 to 1983 composed of three extreme cold coastal events occurring at the same time in the three coastal domains of interest (Figure 3). The coastal warm events in 1984 (February–April) and 1984 (June–September) identified in the OGCM are described as one single event 1984 in the literature (Florenchie et al., 2003, 2004; Lübbecke et al., 2010; Rouault, 2012; Rouault et al., 2003; Shannon et al., 1986). Similarly, the extreme coastal events in 1994 (October–December) and 1995 (February–April) identified with the OGCM are described as one single event occurring in 1994/1995 (December–July) by Rouault (2012). The reason for splitting these two events is based on the abovementioned criteria that are used to identify the different events. Also, Rouault (2012) only used OI-SST in Southern Angola and Northern Namibia for his criteria. Gammelsrød et al. (1998) identified the 1995 event in late austral summer as per our study. Monthly DNT10A indeed drop suddenly in May 1984 (January 1995) and are below +1 STD in the three domains before increasing again in the following month (Figure 3). The study of Lutz et al. (2013), using only SST from the Hadley Centre Sea Ice and Sea Surface Temperature version 1 (Rayner et al., 2003), found a major warm event occurring from January 1963 to March 1964 that is represented in the OGCM as a moderated warm event in 1963/1964 (November–February). The duration of the warm and cold events (Table S1 in the supporting information) varies from a couple of months to half a year or more (for example, the Benguela Niños 1995 and 2010/2011) consistent with findings of Florenchie et al. (2004). The distribution of extreme warm and cold events for the three different coastal domains (not shown) shows that for all the three coastal domains, a maximum of occurrences is observed between March and April. This agrees with previous studies (Florenchie et al., 2004; Lübbecke et al., 2010) which observed that March–April seems to be the peak season for Benguela Niño and Nina interannual events.

3.2. Description of Undocumented Extreme Anomalous Coastal Events

This section is dedicated to the description of some well-known and the newly identified extreme coastal events which occur along the southwestern African coast as presented in section 3.1.

3.2.1. Anomalous Extreme Warm Events

DT10A averaged in February-March-April (FMA) of the three new extreme warm coastal events 1958/1959 (December–July; Figure 4a), 1960/1961 (September–April; Figure 4b), and 1974 (April–July; Figure 4d) are described and intercompared with the 1962/1963 (Figure 4c), 1995 (Figure 4e), and 2011 (Figure 4f) warm events being already documented in the literature.

In late austral summer (FMA) 1959, during the 1958/1959 extreme event (Figure 4a), DT10A along Southern Angola and Northern Namibia are found to be larger than 1 °C. Maximum warm anomalies (DT10A > 2 °C) are found in NBUS up to ~25°S. In January 1959, the peak month of the 1958/1959 Benguela Niño in Southern Angola and ABF (cf. Table S1 in the supporting information), maximum DT10A extend from 11°S to ~22°S with peak values exceeding 3 °C (not shown). This warm anomaly spreads further south (~25°S) in March 1959, while at the same time the warm anomaly decreases in intensity in Southern Angola (<1.5 °C). In April 1959, the warm anomaly is considerably reduced and DT10A greater than 1 °C are observed along the west coast of Africa with another maximum (>2 °C) just north of Angola. During FMA 1961 (Figure 4b), positive DT10A are observed along the West African coast with maximum DT10A (>1 °C) extending from 16°S to ~23°S. The warming pattern extends northward along the African coast and westward, toward, and along the equator up to around 18°W. The 1961 FMA average of DT10A is less intense than the FMA 1959 average (Figure 4a). In January 1961, the peak month of the 1960/1961 Benguela Niño in Southern Angola and ABF (cf. Table S1 in the supporting information), strong DT10A (>2 °C) are present from 12°S up to 18°S (not shown). In February 1961, DT10A peak in Northern Namibia where the warm anomaly is now located from 17°S to 22°S. In April 1961, DT10A vanish north of the ABF along the West African coast and are present in Northern Namibia with less intensity (>0.5 °C).

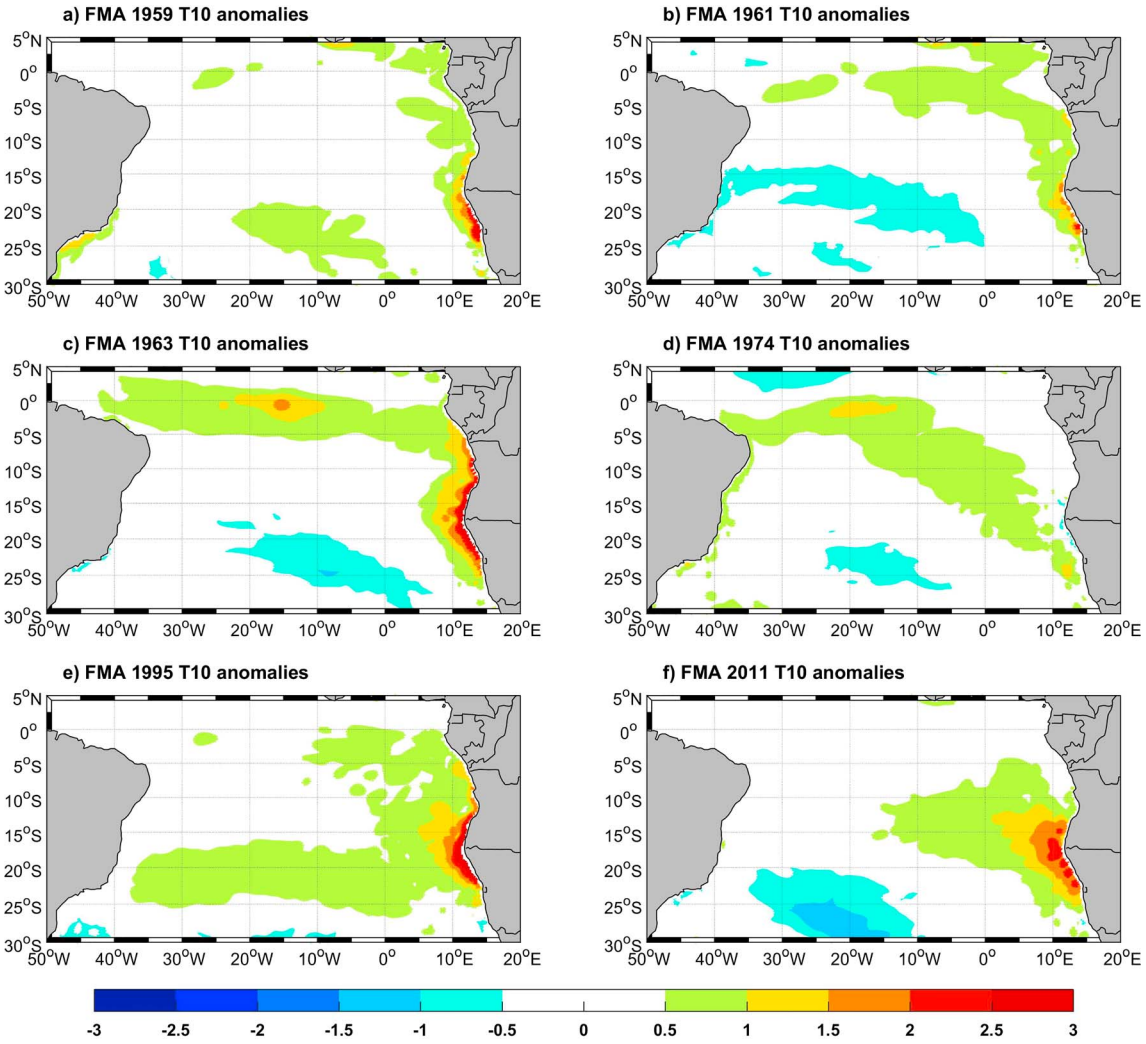

Figure 4. Monthly detrended anomalies of T10 (°C) averaged in February-March-April (FMA) during the Benguela Niño events of (a) 1958/1959, (b) 1960/1961, (c) 1962/1963, (d) 1974, (e) 1995, and (f) 2010/2011.

Figure 4c shows that FMA 1963 is the most intense coastal warm event (Figure 11) even though it peaks around May–June (cf. Table S1 in the supporting information). The maximum warming (>2.5 °C) occurs along the West African coast from Southern Angola up to Northern Namibia reaching a couple of degrees from the coast into the open southeastern Atlantic. Near the equator, a zonal band of warm anomalies (>0.5 °C) extends northwestward from the West African coast toward the Brazilian coast. Katz (1977) observed that zonal wind stress near the equator west of 10°W was anomalously low during the EQUALANT I cruise in 1963 (February–April). Such low zonal wind stress is typically associated with the development of Atlantic Niños or even Benguela Niños (Lübbecke et al., 2010). Maximum DT10A (>3 °C) are observed in May–June along the equatorial waveguide and the West African coast up to 25°S (not shown). This is consistent with the previous study of Stander and De Decker (1969) cited by Shannon et al. (1986) who reported maximum warm anomalies at 20-m depth in June 1963 using station data of temperature around Walvis Bay. Also, Merle (1980) reported that the 1962/1963 extreme warm event was very different from other warm events as it occurred at the time of the Atlantic Niño in the eastern equatorial Atlantic.

Shannon et al. (1986) reported that the water was 5 °C warmer than usual and further suggested an intrusion of Angolan waters along the coast or open ocean waters from the north-west into the NBUS. They concluded that the positive anomalies observed in the NBUS in 1963 were not locally forced. This extreme coastal event is terminated by a cold anomaly of T10 that develops along the Gabon–Congo coastlines in August 1963 (not shown).

21699291, 2019, 8, Downloaded from https://agupubs.onlinelibrary.wiley.com/doi/10.1029/2019JC015013 by Cochrane France, Wiley Online Library on [04/05/2024]. See the Terms and Conditions (https://onlinelibrary.wiley.com/terms-and-conditions) on Wiley Online Library for rules of use; OA articles are governed by the applicable Creative Commons License

21699291, 2019, 8, Downloaded from https://agupubs.onlinelibrary.wiley.com/doi/10.1029/2019JC015013 by Cochrane France, Wiley Online Library on [04/05/2024]. See the Terms and Conditions (https://onlinelibrary.wiley.com/terms-and-conditions) on Wiley Online Library for rules of use; OA articles are governed by the applicable Creative Commons License

The FMA 1974 event (Figure 4d) is different from the previous ones due to the absence of positive DT10A along the Angolan and most of the southwestern African coast. The warming pattern encompassing DT10A greater than 0.5 °C extends northwestward from Northern Namibia up to the central equatorial Atlantic and then westward toward the Brazilian coast. The 1974 extreme coastal event peaks in May in Southern Angola and June in the ABF domain and Northern Namibia (cf. Table S1 in the supporting information). The warming intensifies in May 1974 with DT10A greater than 3 °C extending from 21°S to 0°N along the West African coast and centered in the equatorial Atlantic (not shown). Strong DT10A persist in June 1974 along the equator and the West African coast.

Over the late austral summer season 1995 (Figure 4e), DT10A form an intense warming area (>2 °C) between 13°S and 23°S which is quite similar to the 1963 coastal event (Figure 4c) in the same delimited area. The warming area (>0.5 °C) extends offshore into the open southeastern Atlantic between the African coast and 38°W from 15°S to 25°S. Such warming pattern is not observed for other warm events. The peak of the 1995 warm event is found in March 1995 with a broad band of intense DT10A greater than 3 °C between 12°S and 23°S (not shown). The DT10A decrease in May 1995 shrinking in its extension to the region between 20°S and 23°S. These results are consistent with Rouault et al. (2003) who observed that during the 1995 Benguela Niño, upwelling-favoring winds were reduced and could have contributed to the intensification of the 1995 warm event.

Lastly, Figure 4f shows that during FMA 2011, positive DT10A greater than 1 °C are found in a broad area extending from the coast to couple of degrees offshore between ~25°S and 12°S. Positive anomalies of T10 (>1 °C) appear along the West African coast north of 18°S in October 2010, reach their maximum in December in Southern Angola (>2.5 °C), and propagate southward into the NBUS in February 2011. Rouault et al. (2018) found that the 2010/2011 Benguela Niño started along the Angolan coast in November 2010 and peaked in January 2011. DT10A persist up to April 2011, when the warm event is terminated by a cold event in May 2011 consistent with the results of Rouault et al. (2018). Rouault et al. (2018) reported that the weakening of easterly winds in the western equatorial Atlantic in October 2010 triggered a downwelling IEKW at the origin of the 2010/2011 Benguela Niño. Across the ABF, a strong poleward flow developed and advected warm tropical water into Northern Namibia (Rouault et al., 2018).

3.2.2. Anomalous Extreme Cold Events

Figure 5 is similar to Figure 4 but for four extreme cold coastal events in FMA 1981, 1985, 1992, and 1997. Figures in the first row are the newly identified extreme cold events (Figures 5a and 5b).

The 1965 extreme cold event is not displayed with the others because it occurs from October to December. It is a short coastal event. It peaks in October 1965 in Southern Angola and in November 1965 in the ABF domain with substantial detrended anomalies of T10 (<−2 °C) close to the southwestern African coast between 7°S and 19°S. Colder than usual DT10A are not observed in the Northern Namibia domain.

The area of cold DT10A observed in FMA 1981 (Figure 5a) extends northwestward toward the Brazilian coast. Cold DT10A (<−1 °C) are present in Southern Angola. In February 1981, strong negative anomalies of T10 (<−1 °C) are observed along the Northern Namibia coast (not shown). Cold DT10A progress northward along the Southern Angolan coast in March 1981 and extend to Northern Angola in April 1981 (not shown).

In FMA 1985 (Figure 5b), cold DT10A (<−0.5 °C) are observed between Southern Angola and Northern Namibia. Cold DT10A appear in March 1985 mostly in a broad area south of 10°S with a minimum (<−1.5 °C) observed along the Northern Namibia coast, while cold anomalies are present farther north in April 1985 from 4°S toward Northern Namibia (not shown). In May 1985, cold DT10A persist in the southeastern Atlantic Ocean and disappear in August 1985 with the presence of warm DT10A along the West African coast (not shown).

During late austral summer 1992 (Figure 5c), minimum DT10A (<−1 °C) are confined to the West African coast between 6°S and 22°S. In December 1991, cold DT10A (<−1.5 °C) are present along the coast from 2°S to 15°S. In February 1992, cold DT10A propagate poleward along the West African coast and are visible around 23°S before peaking in March 1992 with DT10A of ~−2.5 °C found between Southern Angola and Northern Namibia. The patch of cold anomalies extends from the coast to 30°W. Cold DT10A persist along the West African coast until August 1992 (not shown).

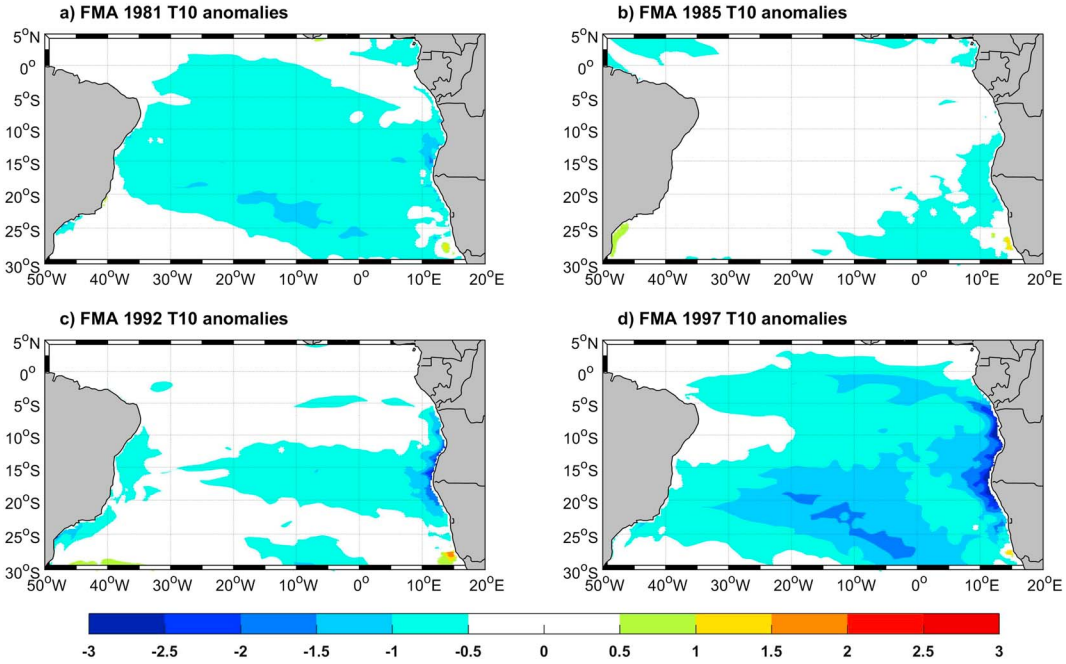

Figure 5. Monthly detrended anomalies of T10 (°C) averaged in February-March-April (FMA) during the Benguela Niña events of (a) 1981, (b) 1985, (c) 1991/1992, and (d) 1996/1997.

In FMA 1997 (Figure 5d), an intense cold T10 anomaly covers almost the entire South Atlantic reaching values less than −3 °C along the West African coast from 5°S to 22°S. Note that the 1996/1997 cold event is the coldest event observed over the 1958–2015 period (Figures 3 and 11). The 1996/1997 extreme cold event reaches its mature phase in April 1997 in the three coastal domains of interest (cf. Table S1 in the supporting information). This is consistent with the study of Florenchie et al. (2004). The following section will focus on the triggering processes associated with Benguela Niño and Niña events.

3.3. Origin of the Anomalous Coastal Events

3.3.1. Equatorial Remote Forcing

The OLM outputs are used to investigate the equatorial origin of the anomalous coastal events from 1958 to 2015. In this study, we use the same equatorial domain as Imbol Koungue et al. (2017) to characterize the IEKW propagations along the equatorial Atlantic. Figure 6 depicts the first three baroclinic mode IEKW averaged along the equator between 20°W and 0°E (Imbol Koungue et al., 2017). The colored rectangles represent the anomalous coastal events identified in Figure 3. Positive (negative) detrended anomalies of IEKW represent downwelling (upwelling) IEKW. We notice that most of the coastal warm (cold) coastal events are preceded by the propagation of downwelling (upwelling) IEKW. This means that the remote equatorial forcing is at the origin of most of the coastal anomalous events in the Angola-Benguela upwelling system. This is in good agreement with the recent study of Imbol Koungue et al. (2017) which used PIRATA, AVISO, and the same OLM to track the IEKW from 1998 to 2012. Figure 6 also shows that the second-mode IEKW (in blue) is the dominant mode of IEKW along the equatorial Atlantic (Illig et al., 2004; Imbol Koungue et al., 2017). For example, the OLM outputs show that a second-mode downwelling IEKW propagates along the equator about one month before the extreme warm coastal event 1962/1963 (Figure 6a) occurred in the Angola-Benguela upwelling system. Therefore, remote forcing via propagation of downwelling IEKW mode 2 could have triggered the 1963 Benguela Niño reported by Shannon et al. (1986). All the new extreme warm coastal events (1958/1959, 1960/1961, and 1974) are associated with the propagation of a downwelling IEKW mode 2 along the equator. The 1995 extreme coastal warm event is also associated with the propagation of a downwelling IEKW mode 2 along the equator during its onset.

Figure 6b shows that a downwelling IEKW mode 2 with an amplitude of ~1.5 cm propagates along the equator in September 2010 and is linked to the 2010/2011 extreme event. This is consistent with the study of

21699291, 2019, 8, Downloaded from https://agupubs.onlinelibrary.wiley.com/doi/10.1029/2019JC015013 by Cochrane France, Wiley Online Library on [04/05/2024]. See the Terms and Conditions (https://onlinelibrary.wiley.com/terms-and-conditions) on Wiley Online Library for rules of use; OA articles are governed by the applicable Creative Commons License

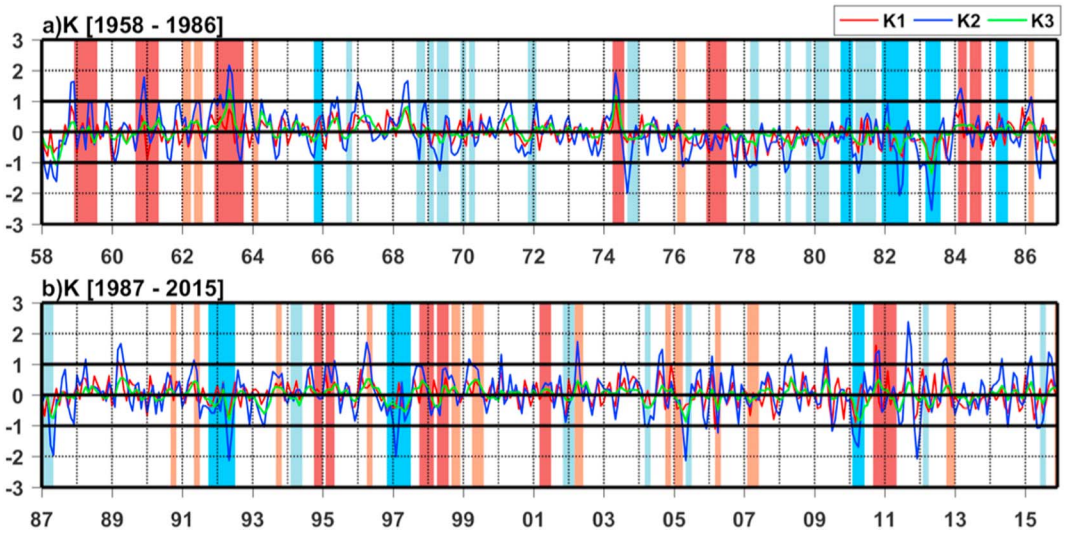

Figure 6. Monthly OLM detrended anomalies from (a) 1958 to 1986 and (b) 1987 to 2015 of the gravest IEKW modal contributions to SSHA (cm) at 0°N averaged over (20°W–0°E): first (K1), second (K2), and third (K3) mode are in red, blue, and green, respectively. Red and blue rectangles represent the extreme and moderate coastal warm and cold events identified in Figure 3.

Rouault et al. (2018). Conversely, the onsets of the newly identified extreme cold events (1965, 1980/1981, and 1985) are associated with upwelling IEKW mode 2 of low-amplitude recorded along the equatorial Atlantic (Figure 6a). Some extreme coastal events seem to be locally forced, for example, the coastal warm event in 1976/1977 which occurs concomitantly with the propagation of an upwelling IEKW mode 2 (Figure 6a). More details regarding the local processes and this extreme coastal warm event will be given in section 3.3.3.

Highly statistically significant correlations at 95% of around 0.5 are found when the index of IEKW mode 2 (represented in blue in Figures 6a and 6b) leads the DNT10A in the Southern Angola and ABF domains by one month (lag −1), as observed in Figures 7a and 7b. Similar results are found for anomalies of T10 in Northern Namibia and the index of IEKW mode 2 but with a correlation of ~0.4 at lag −1 (Figure 7c). These significant correlations show the importance of IEKW mode 2 for initiating warm and cold events in the Angola-Benguela upwelling system at one-month lag. Similar results were found by Imbol Koungue et al. (2017). Also, we note from Figures 7a–7c, statistically significant correlations at 95% occurring at a broad lag interval ranging from zero to three (zero to seven) months when the second-mode IEKW index leads DNT10A in the Southern Angola and ABF (Northern Namibia). Along the Angola-Namibia coastline, the zero- to three-month lags might be associated with the duration of the coastal events or also explained by the contribution of distinct baroclinic modes that can differ from one event to another and which contribution is controlled by the southeastern Atlantic stratification variability (Imbol Koungue et al., 2017). Lags greater than three months observed in the Northern Namibia domain could be attributed to the slow advection of warm tropical waters from Southern Angola to Northern Namibia (Rouault, 2012).

3.3.2. Large-Scale Wind Stress Forcing

To better understand the relation between Benguela Niños/Niñas, SST, and wind stress in the tropical Atlantic, a lagged composite analysis of detrended anomalies of T10 and wind stress over the tropical Atlantic domain (50°W–20°E, 30°S–20°N) is performed. Only results for extreme coastal warm or cold events are presented here as they are more representative of Benguela Niño and Niña events. Compositing is done by selecting all the extreme warm and cold coastal events summarized in Table S1 in the supporting information which peak in March or April for at least two coastal domains of interest (cf. section 2.3.6). The wind stress anomaly composites derive from the same method, using extreme warm and cold event peaks identified using the DNT10A. Four extreme warm coastal events (1976/1977, 1984, 1995, and 2001) and four extreme cold coastal events (1981/1982, 1985, 1991/1992, and 1996/1997) are selected. Lagged composite of T10 and wind stress anomalies maps are presented in Figures 8 and 9, with a lag interval ranging from three

21699291, 2019, 8, Downloaded from https://agupubs.onlinelibrary.wiley.com/doi/10.1029/2019JC015013 by Cochrane France, Wiley Online Library on [04/05/2024]. See the Terms and Conditions (https://onlinelibrary.wiley.com/terms-and-conditions) on Wiley Online Library for rules of use; OA articles are governed by the applicable Creative Commons License

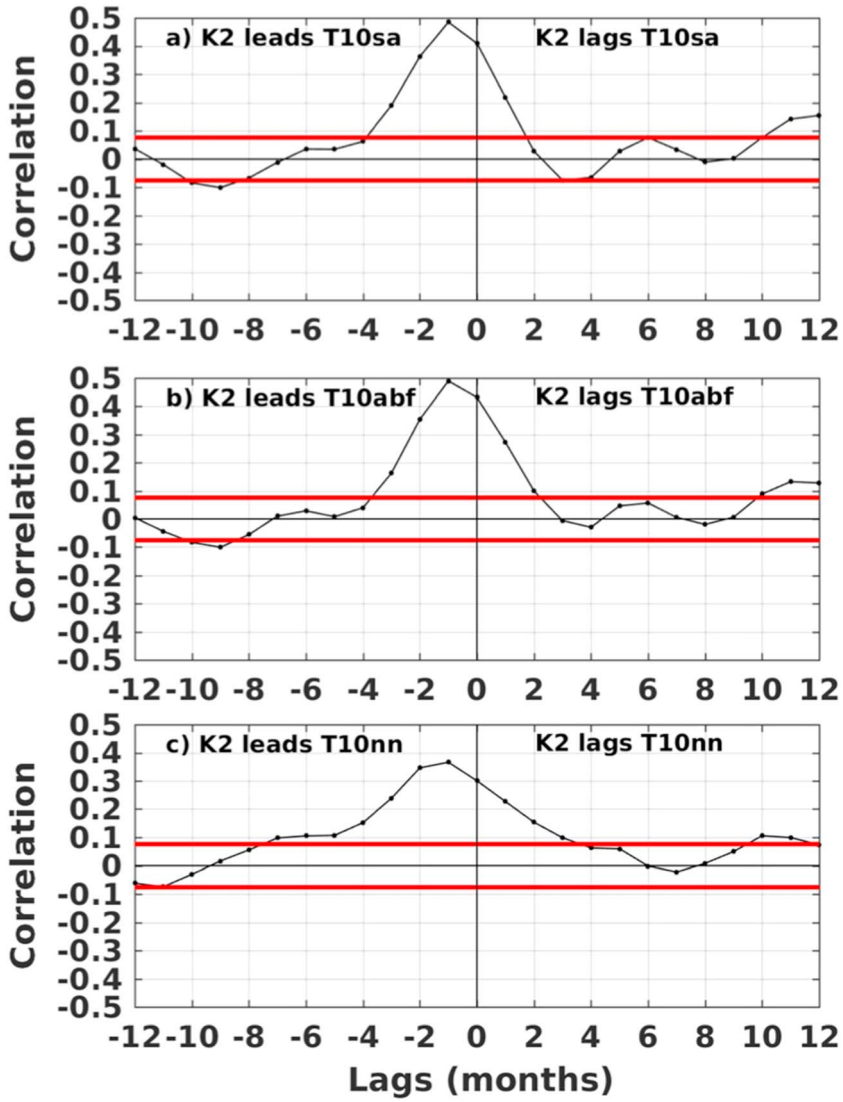

Figure 7. Correlation analysis over 1958–2015 between monthly detrended normalized OLM IEKW second mode SSHA (K2) averaged between 20°W and 0°E at 0°N and DNT10A along the African coast (averaged within the 1°-width coastal fringe) in (a) Southern Angola (T10sa; averaged between 10°S and 15°S), (b) ABF domain (T10abf; averaged between 15°S and 19°S), and (c) Northern Namibia (T10nn; averaged between 19°S and 24°S) in function of the lag (in months). Negative lags indicate that K2 leads the coastal T10 variability. Correlations statistically significant at 95% are found outside the correlation thresholds (using *p* value statistical test from Sciremammano (1979)) which are indicated by thick red lines.

months before the peak of the event to two months after the peak. Three months before the peak (Figure 8a), there is no significant warming along the coasts of Angola and Namibia. Northeasterly wind stress anomalies are present in the western part of the equatorial Atlantic. Two months before the peak (Figure 8b), the pattern of DT10A exhibits a meridional dipole of DT10A with a positive (>0.5 °C) anomaly observed along the southwestern coast of Africa up to 18°S and a minimum DT10A (<−0.5 °C) observed in the northern tropical Atlantic along the Mauritania–Senegalese coastlines. The wind stress anomaly coverage comprises concomitantly westerly wind stress anomalies along the equator east of 30°W, northwesterly wind stress anomalies between the equator and 10°S, northerly wind stress anomalies which start to be noticeable close to the western African coast up to 10°S, and weak wind stress pattern associated with the SAA from 40°W to 10°E south of 15°S. This large-scale weak wind stress anomaly pattern suggests a basin-scale weakening of the SAA. This composite analysis is suggestive of a link between the wind stress anomalies in the subtropical South Atlantic

21699291, 2019, 8, Downloaded from https://agupubs.onlinelibrary.wiley.com/doi/10.1029/2019JC015013 by Cochrane France, Wiley Online Library on [04/05/2024]. See the Terms and Conditions (https://onlinelibrary.wiley.com/terms-and-conditions) on Wiley Online Library for rules of use; OA articles are governed by the applicable Creative Commons License

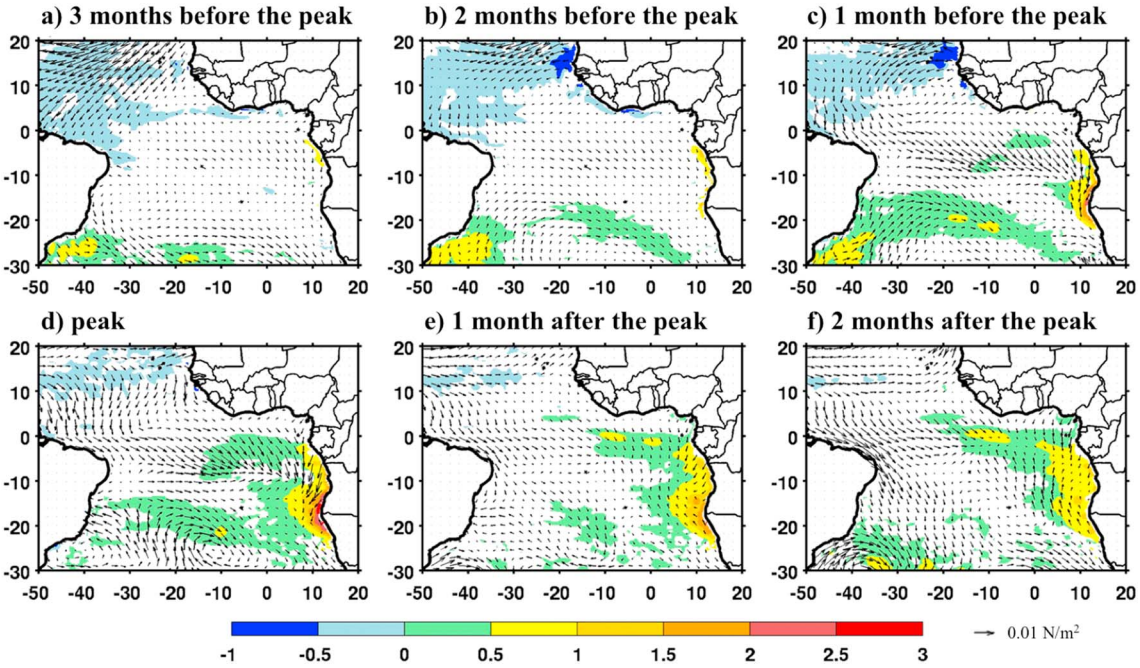

Figure 8. Composite maps of detrended anomalies of T10 (in color; in °C) and surface wind stress (arrows; N/m^2) computed from four selected extreme warm coastal events (1976/1977, 1984, 1995, and 2001) and averaged during (a) December–January (three months before peak), (b) January–February (two months before the peak), (c) February–March (one month before the peak), (d) March–April (peak), (e) April–May (one month after the peak), and May–June (two months after the peak). The shaded areas (detrended anomalies of T10) represent the 90% statistically significant areas.

in January–February (two months before the peak) and a warming in the Angola-Benguela upwelling system which agrees with Lübbecke et al. (2010) and Richter et al. (2010). The equatorial wind stress anomalies observed in the central equatorial Atlantic zone have been already shown to be important to force the IEKW (Imbol Koungue et al., 2017).

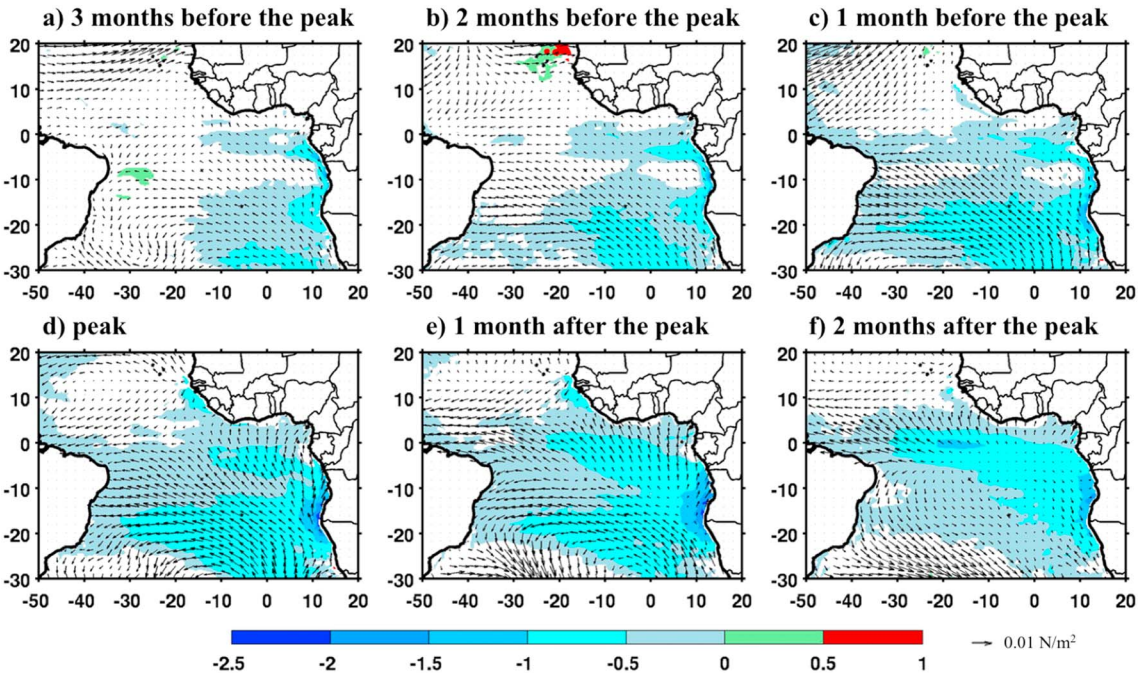

Figure 9. Same as in Figure 10 but for the composites of four extreme cold coastal events (1981/1982, 1985, 1991/1992, and 1996/1997).

21699291, 2019, 8, Downloaded from https://agupubs.onlinelibrary.wiley.com/doi/10.1029/2019JC015013 by Cochrane France, Wiley Online Library on [04/05/2024]. See the Terms and Conditions (https://onlinelibrary.wiley.com/terms-and-conditions) on Wiley Online Library for rules of use; OA articles are governed by the applicable Creative Commons License

21699291, 2019, 8, Downloaded from https://agupubs.onlinelibrary.wiley.com/doi/10.1029/2019JC015013 by Cochrane France, Wiley Online Library on [04/05/2024]. See the Terms and Conditions (https://onlinelibrary.wiley.com/terms-and-conditions) on Wiley Online Library for rules of use; OA articles are governed by the applicable Creative Commons License

One month before the peak (Figure 8c), the signature of the Benguela Niño is quite well observed from 5°S to 22°S with the maximum (>2 °C) found between Southern Angola and the position of ABF (~17°S). The coastal warming extends from the West African coast to ~3° offshore. The large-scale weakening of the SAA intensifies and is now well developed. Concomitantly, south of the equator, the presence of northerly wind stress anomalies observed north of 20°S along the southwestern African coast would favor an intensification of the coastal warming of the Benguela Niño, which will be discussed further. It suggests that during the onset of Benguela Niño events, both local and remote forcing could act concomitantly as part of the same large-scale wind stress anomaly pattern. The potential role of the local forcing during the onset of the Benguela Niño events will be investigated in section 3.3.3. However, northwesterly wind stress anomalies (weakened southeasterly trade winds) observed south of the equator up to ~10°S, east of 20°W over the warming area might be indicative of an ocean–atmosphere coupling, through the wind-evaporation-SST (WES) feedback (Lübbecke et al., 2010), that could contribute to amplify the weakening of the southerly wind stress along the Angolan coast. Also note that this region comprises the region where CTWs are forced by wind stress fluctuations as highlighted by Bachèlery et al. (2016). This will also be investigated in section 3.3.3.

During the peak of the extreme warm coastal events occurring in March–April (Figure 8d), the signature of Benguela Niño is well developed with a maximum T10 anomaly of ~3 °C between 15°S and 18°S along the Angolan and Namibian coastline. Warm DT10A extend further south continuously up to around 25°S, corresponding to the approximate maximum latitude where the signature of Benguela Niños and corresponding interannual CTWs can be tracked (Bachèlery et al., 2016). The warm T10 anomaly with values greater than 0.5 °C extends northwestward into the eastern equatorial Atlantic region up to 15°W, a region with a strong seasonal cycle of SST (the seasonal formation of the Atlantic Cold Tongue) which is modulated interannually by the so-called Atlantic Equatorial Mode often referred to Atlantic Niño with peak variability in Austral winter (Jouanno et al., 2011, 2017; Lübbecke et al., 2010). The wind stress anomalies during the mature phase of the selected extreme events reveal persisting northerly anomalies over the warm areas along the Angolan coast. A convergence of weakened wind stress anomalies is observed over the warm area around 10°S which is also observed in Figure 8c. This could be explained by the coupling mechanism proposed by Hu and Huang (2007). According to Hu and Huang (2007), coastal warming observed in austral fall in the southern tropical and equatorial Atlantic seems to trigger wind convergence associated with westerly wind stress anomalies to the west of the warm anomaly. The basin-scale weakening of the SAA persists during the peak of the extreme warm event.

One month after the peak (Figure 8e), a similar warm pattern is observed as in Figure 8d close to the Southern Angola and Northern Namibia coastlines, but with less intensity. This suggests the demise of the extreme warm coastal event. Westerly wind stress anomalies are still observed in the western part of the equatorial Atlantic. The intensity of the warming pattern observed in Figure 8e decreases along Southern Angola and Northern Namibia 2 months after the peak (Figure 8f), but the warming spreads northwestward along the equatorial Atlantic. This suggests that an Atlantic Niño is developing over the eastern equatorial Atlantic, which is consistent with the tendency of the Atlantic Niños to occur after Benguela Niños (Lübbecke et al., 2010; Richter et al., 2010; Rouault et al., 2009). Indeed, according to Lübbecke et al. (2010), there is a season lag between Benguela Niños and Atlantic Niños. Also, the presence of the westerly wind stress anomalies in the western equatorial Atlantic two months after the peak (May–June) could trigger a downwelling IEKW mode 2 which would deepen the thermocline in the eastern equatorial Atlantic favoring the onset of Atlantic Niño in the eastern equatorial Atlantic in austral winter (Hormann & Brandt, 2009; Lübbecke et al., 2010).

Figure 9 presents the same analysis as Figure 8 but for the four extreme cold events mentioned above (1981/1982, 1985, 1991/1992, and 1996/1997). Compared to the extreme warm event composite maps (Figure 8), the area of 90% statistically significant cold anomalies is much broader and covers the South Atlantic for some cases (Figures 9b–9f). The composite maps do not portray the meridional dipole pattern of DT10A depicted in Figure 8 as no warming pattern is present in the northern tropical Atlantic except in Figure 9b.

Three months before the peak of the Benguela Niñas (Figure 9a), cold anomalies appear east of 20°W south of the equator with minimum DT10A (<−0.5 °C) observed between 20°S and 0°S. Two months before the peak (Figure 9b), the cold anomalies start spreading along the equator and westward into the open South Atlantic.

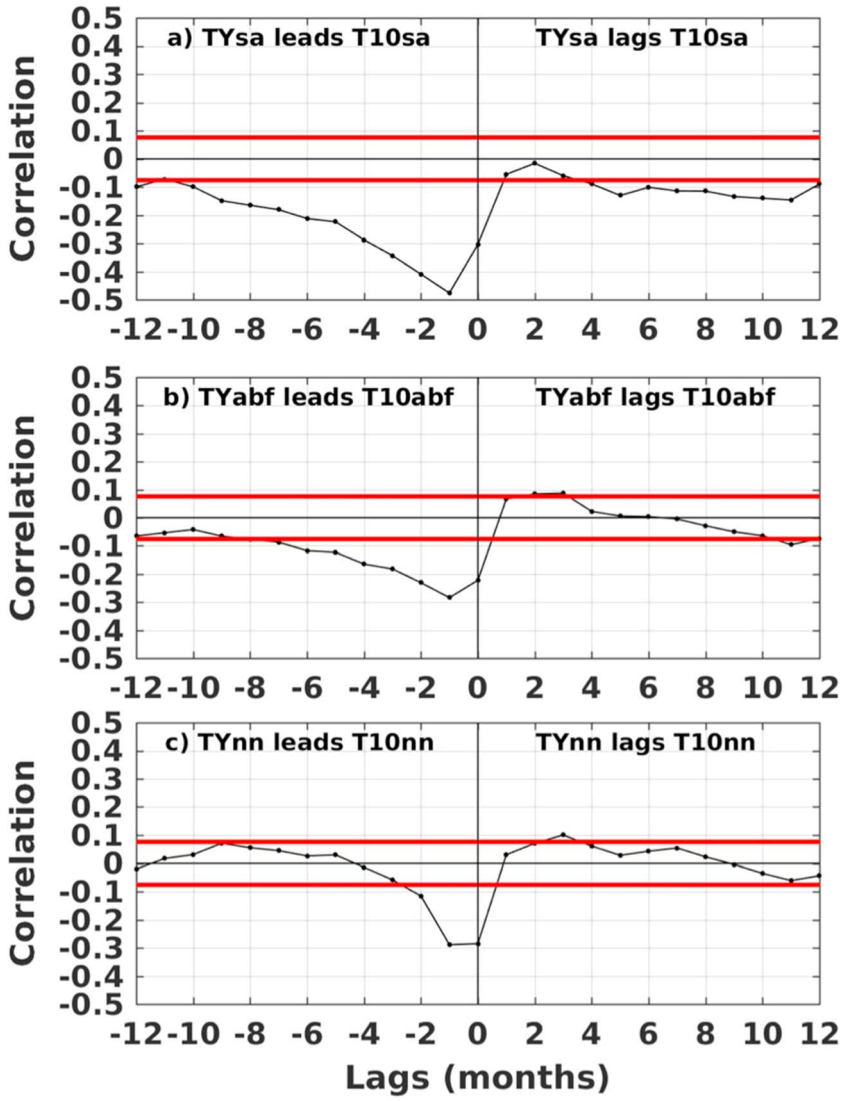

Figure 10. Local correlation analysis over 1958–2015 between coastal (averaged within the 1°-width coastal fringe) monthly detrended normalized anomalies of DFS5.2 surface meridional wind stress (TY) and OGCM T10 anomalies in (a) Southern Angola (sa; averaged between 10°S and 15°S), (b) ABF domain (abf; averaged between 15°S and 19°S), and (c) Northern Namibia (nn; averaged from 19°S to 24°S) in function of the lag (in months). Negative lags indicate that TY leads the T10 variability. Correlations statistically significant at 95% are found outside the correlation thresholds (using *p* value statistical test from Sciremammano (1979)) which are indicated by thick red lines.

At the same time, southerly wind stress anomalies start to develop over the cold anomalies. Strong southeasterly wind stress anomalies are present south of the equator between 25°S and 5°S and from 20°W to 10°E. These strong southeasterly wind stress anomalies are part of the wind stress pattern that strengthen the SAA and are occurring above the large cooling pattern. One month before the peak, Figure 9c reveals cold DT10A along the equatorial Atlantic almost connected with the cooling in the South Atlantic. There is evidence of basin-scale strengthening of the wind stress over the tropical Atlantic. Easterly wind stress anomalies observed in the western equatorial Atlantic are quite well connected with the southeasterly wind stress anomalies located over the cold DT10A. These wind stress anomalies form the northeastern part of the anticyclonic circulation present south of 20°S in the southern tropic attributed to the SAA. The SAA seems to have intensified compared to Figure 9b. Along the African coast, southerly wind stress anomalies are present over the cold anomalies and south of it. Similar to the Benguela Niño composite (Figure 10c), the WES feedback might be at work, explaining the intensification of the southeasterly wind stress north of 10°S. The WES feedback resulting in the amplification of the weak

21699291, 2019, 8, Downloaded from https://agupubs.onlinelibrary.wiley.com/doi/10.1029/2019JC015013 by Cochrane France, Wiley Online Library on [04/05/2024]. See the Terms and Conditions (https://onlinelibrary.wiley.com/terms-and-conditions) on Wiley Online Library for rules of use; OA articles are governed by the applicable Creative Commons License

21699291, 2019, 8, Downloaded from https://agupubs.onlinelibrary.wiley.com/doi/10.1029/2019JC015013 by Cochrane France, Wiley Online Library on [04/05/2024]. See the Terms and Conditions (https://onlinelibrary.wiley.com/terms-and-conditions) on Wiley Online Library for rules of use; OA articles are governed by the applicable Creative Commons License

(strong) southeasterly wind stress observed south of the equator up to ~10°S, east of 20°W over the significant warming (cooling) area one month before the peak of a Benguela Niño (Niña), seems to be more active in Figure 10c (Figure 11c). This could suggest an asymmetric WES feedback during the onset of a Benguela Niño (Niña) event.

During the peak (March–April; Figure 11d), the Benguela Niña is at its mature phase. Minimum DT10A (<−1 °C) are present between 22°S and 3°S along the West African coast. Cold DT10A cover most of the tropical South Atlantic. A similar widespread warm anomaly is not observed during the extreme Benguela Niño events. Our results suggest an asymmetry of Benguela Niños/Niñas. We observe southerly wind stress anomalies over the cooling area along Angolan coast up to the ABF zone (~17°S). Concomitantly, strong southeasterly wind stress anomalies offshore up to 30°W which gain a strong zonal component and become easterly wind stress anomalies toward the Brazilian coast and easterly wind stress anomalies in the western part of the equatorial Atlantic are observed. These strong wind stress anomalies suggest a strengthening of the large-scale atmospheric circulation.

On month after the peak (Figure 9e) coastal cooling of Angola and Namibia persists and broadens, but with less intensity compared to the cooling depicted in Figure 9d. This suggests that a Benguela Niña event lasts longer than a Benguela Niño event, which agrees with the findings of Florenchie et al. (2004) based on SST observations. In terms of wind stress anomalies, basin-scale strengthening of wind stress persists over the South Atlantic. South of the equator, an anticyclonic atmospheric circulation is well developed and seems to have shifted northward prior to the development of the Atlantic cold tongue along the equatorial Atlantic in austral winter (Jouanno et al., 2011). Easterly wind stress anomalies are reduced over the equatorial Atlantic, still present west of 20°W. This could be linked to the onset of the Atlantic cold tongue which appears in austral winter in the eastern part of the equatorial Atlantic (Jouanno et al., 2011) concomitantly with the SAA located farther north. Cross-equatorial southerly wind anomalies are present in the Gulf of Guinea east of 10°W and will lead to more cooling along the equatorial Atlantic through upwelling, entrainment, and evaporation processes (Okumura & Xie, 2004). For the Angola–Benguela Current system, southerly wind stress anomalies are still observed along the Angolan coast (Figures 9d and 9e).

Two months after the peak of Benguela Niña (Figure 9f), cold DT10A are reduced over the tropical Atlantic. The demise of the Benguela Niña along the coast of Angola and Namibia is remarkable. Similarly, to Figure 8 f, cold DT10A (<−0.5 °C) spread westward along the equatorial Atlantic marking the onset of the Atlantic cold tongue (Jouanno et al., 2011). According to Jouanno et al. (2011), the cooling in the eastern equatorial Atlantic observed in May–June happens in phase with the rise of the thermocline in this area due to the strengthening of the easterlies in the western equatorial Atlantic as observed in Figure 9f. Strong southeasterly and cross-equatorial southerly wind stress anomalies are found on the northern flank of the Atlantic cold tongue, whereas the wind stress is weaker than its seasonal average on its southern flank. There is a convergence of the wind stress anomalies around 10°N which is fed by strong cross-equatorial southerly wind stress anomalies present on the northern flank of the Atlantic cold tongue. The wind stress anomalies following the shape of the SAA extend into the southwestern tropical Atlantic but are considerably weakened at the southeastern side over cold waters.

3.3.3. Potential Role of Local Atmospheric Forcing

We have previously seen that both (local and remote) forcing could act simultaneously during the onset of a Benguela Niño and Niña. Generally, along the southwestern African coast, alongshore wind stress strengthens seaward leading to a cyclonic or negative wind stress curl (Bakun & Nelson, 1991; Junker et al., 2015). While the alongshore wind stress directly impacts offshore Ekman transport and coastal upwelling, the impact of the cyclonic wind stress curl that persists throughout the year is more complex. Depending on the distance of the zero-wind-stress-curl contour from the coast (~450 km; not shown), it can drive the poleward undercurrent which may reach the surface (see, e.g., Fennel et al., 2012). The resulting poleward undercurrent will advect warm tropical waters from Angolan to Namibian upwelling region. Therefore, a stronger (weaker) alongshore wind stress that lead to higher (lower) cyclonic wind stress curl and stronger (weaker) poleward undercurrent results into a warming (cooling) downstream. Additionally, a stronger (weaker) alongshore wind speed leads to increased cooling (warming) due to stronger (weaker) turbulent latent and sensible heat loss by the ocean to the atmosphere at the sea surface (see, e.g., Lübbecke et al., 2019).

21699291, 2019, 8, Downloaded from https://agupubs.onlinelibrary.wiley.com/doi/10.1029/2019JC015013 by Cochrane France, Wiley Online Library on [04/05/2024]. See the Terms and Conditions (https://onlinelibrary.wiley.com/terms-and-conditions) on Wiley Online Library for rules of use; OA articles are governed by the applicable Creative Commons License

Figure 10 shows the lag correlation analysis between detrended normalized (using method 1; cf. section 2.3.2) anomalies of collocated meridional wind stress (TY) and T10 in the three domains of interest, respectively. For the period 1958 to 2015, an anticorrelation of around −0.5 (−0.3), statistically significant at 95%, occurs when the local meridional wind stress anomalies lead the DT10A by one month in Southern Angola (ABF domain) as shown in Figure 10a (Figure 10b). In Northern Namibia, statistically significant anticorrelation of −0.3 is found from lags 0 to 1 month when the meridional wind stress anomalies lead DT10A (Figure 10c). This is expected in an upwelling region where coastal ocean responds rapidly to upwelling-favoring wind stress. This is also confirmed in the Southern Namibia upwelling region (25°S to 30°S), where the meridional wind stress anomalies and DT10A are strongly anticorrelated (~−0.56) at lag 0 (not shown). Locally, the weakening (strengthening) of the alongshore wind stress referring to negative (positive) meridional wind stress anomalies occur mostly one month before the onset of the warming (cooling) along the southwestern African coast. This means that the local alongshore wind stress would be in phase with the onset of the coastal event and would enhance and favor the signature of temperature at 10 m of the coastal event. However, warming (cooling) in the nonupwelling-favoring wind areas such as Southern Angola and part of ABF domain could result in a lower (higher) latent heat loss from the ocean to the atmosphere due to weaker (stronger) wind speed.

The highest, statistically significant correlations between DT10A in the Southern Angola domain and IEKW mode 2 (Figure 7a) and local meridional wind stress (Figure 10a) are about the same (0.5). This suggests the concomitant acting role of both forcings as part of the large-scale wind forcing one month before the onset of the coastal event which is also illustrated in Figures 8c and 9c.

Figure 11 shows the normalized intensities calculated as the sum of detrended normalized interannual anomalies for each of the three parameters (T10, IEKW mode 2, and alongshore wind stress) over the period during which each of the 21 extreme coastal events is recorded in the three coastal domains of interest. Note that the time series of detrended normalized anomalies of IEKW mode 2 and meridional wind stress are shifted forward by one month to be in advance of the DT10A (Figures 7 and 10, respectively) before computing their respective intensities. The 21 extreme coastal events are sorted from the warmest to the coolest in the three coastal domains of interest (Figure 11, red line) and show that, over the 1958–2015 period, the warmest coastal event is 1962/1963 (December–September) and the coolest coastal events are 1981/1982 (December–August) and 1996/1997 (November–June), respectively. Indeed, the use of time series of SSTA from the Hadley Centre Sea Ice and Sea Surface Temperature version 1 reanalysis product (Rayner et al., 2003) gives similar conclusions as the one drawn analyzing the OGCM outputs. For most of the coastal event cases, positive or negative intensities of DT10A are associated with positive or negative intensities of IEKW mode 2 anomalies, concomitantly with negative or positive intensities of local meridional wind stress anomalies along the West African coast, respectively. For example, it is the case for the 1958/1959, 1960/1961, and 1974 undocumented Benguela Niño events which are linked to positive intensity of IEKW mode 2 (downwelling equatorial Kelvin wave) and a negative anomaly of local meridional wind stress (alongshore wind stress weaker than the seasonal average) observed one month before the onset of the extreme warm events. Conversely, the 1965, 1980/1981, and 1985 undocumented Benguela Niña events are associated with negative intensity of IEKW mode 2 (upwelling equatorial Kelvin wave) and a positive anomaly of local meridional wind stress (alongshore wind stress stronger than the seasonal average), both forcing observed one month before the onset of the extreme cold events. Similar conclusions are observed for the well-known Benguela Niños that occurred in 1995, 1997/1998, 2010/2011, and 1991/1992 or 1996/1997 Benguela Niña events. However, the 1962/1963 Benguela Niño is associated with a strong downwelling IEKW mode 2 (normalized intensity of 9.9) and northerly wind stress anomalies in the Southern Angola domain (Figure 11, top panel). This weak alongshore wind stress might enhance the local warming in Southern Angola and ABF domain due to reduced ocean heat loss though they strengthen in the southward direction particularly in the Northern Namibia domains (Figure 11, bottom panel), but their amplitude is still low. During the extreme warm coastal event in 1976/1977 (December–June), weaker than normal wind stress is present (normalized intensity of ~−6.2) in Southern Angola (Figure 11, top panel). Surprisingly, this extreme warm coastal event is associated with an upwelling IEKW mode 2 with a normalized intensity ranging between −2 and −1. It means that the 1976/1977 extreme warm event might not have an equatorial origin and could have been locally forced in Southern Angola since alongshore wind stress is weaker than usual which could induce

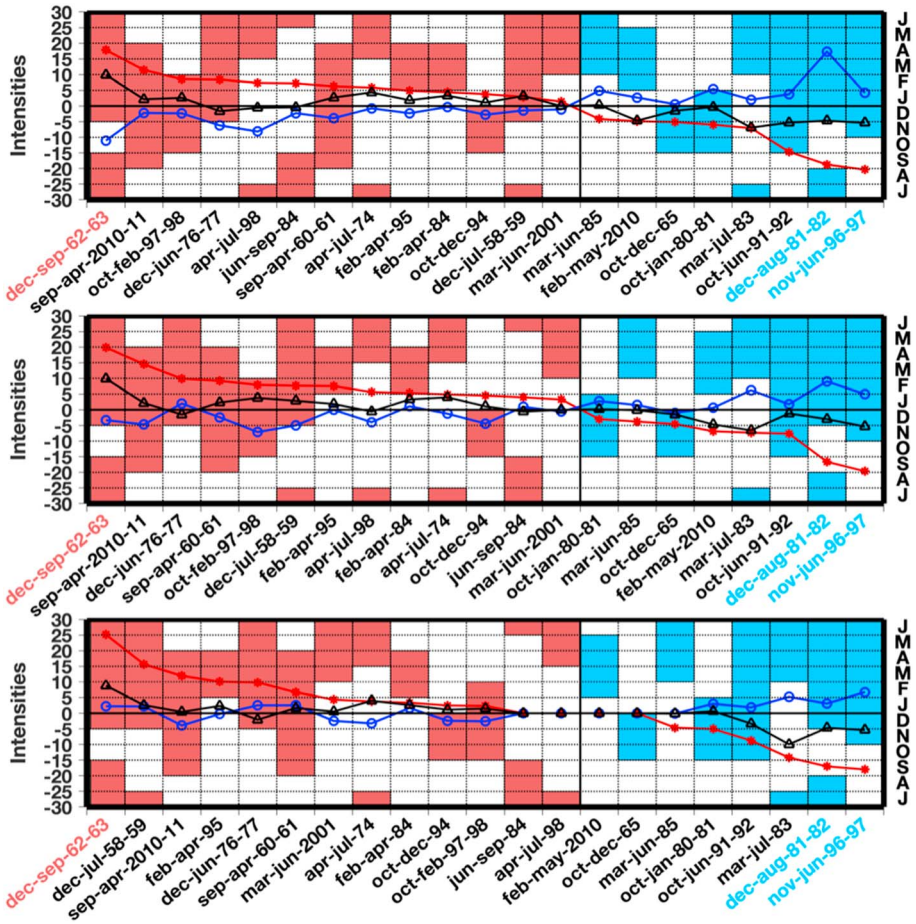

Figure 11. Classification of the coastal events from the warmest to the coolest using DNT10A (averaged within the 1°-width coastal band) from 1958 to 2015 in (top panel) Southern Angola (10°S–15°S), (middle panel) ABF domain (15°S–19°S), and (bottom panel) Northern Namibia (19°S–24°S). Colored tiles highlight to the period during which the coastal temperature anomalies exceed ±1 STD (right *y* axis). The black vertical line separates the warm from the cold events. The labels in red (blue) highlight the warmest (coolest) coastal events observed in the three coastal domains. The dotted red line depicts the normalized intensities of DNT10A at the peak month of each coastal event. The black line with triangles represents the normalized intensities of detrended normalized anomalies of OLM IEKW mode 2 (averaged within (20°W–0°E, 0°N)) shifted forward by one month (to lead T10 by one month, in agreement with Figure 6). The blue line with open circles represents the normalized intensities of detrended normalized anomalies of DFS5.2 surface coastal meridional wind stress (averaged within the same domain as T10) shifted forward by one month (in order to lead T10 by one month, in agreement with Figure 7).

warming due to the reduction of turbulent latent heat loss. DT10A are then advected poleward across the ABF up to 24°S (not shown).

Table 1 shows statistically significant correlation values at 95% between the different normalized intensities shown in Figure 11 in the three coastal domains of interest. In Northern Namibia, there is an anticorrelation of −0.42 between the intensity of detrended normalized anomalies of T10 and local meridional wind stress (TY; Table 1, first row). This could be explained by the fact that the Northern Namibia domain is a more dynamic upwelling zone than the Southern Angola and ABF domains. This makes the identification of anomalous events difficult in Northern Namibia. For example, out of 21 total extreme events, only 17 were recorded in Northern Namibia (see Tables S1 and S2 in the supporting information). Correlation coefficients of ~0.8 confirm the strong link between intensities of detrended normalized anomalies of IEKW mode 2 along the equatorial Atlantic and T10 in the three coastal domains of interest one month before the onset of extreme coastal events (Table 1, second row). This confirms the results discussed in Figures 6 and 7. We also notice that in Southern Angola (Table 1, second row), correlations between intensities of detrended normalized

21699291, 2019, 8, Downloaded from https://agupubs.onlinelibrary.wiley.com/doi/10.1029/2019JC015013 by Cochrane France, Wiley Online Library on [04/05/2024]. See the Terms and Conditions (https://onlinelibrary.wiley.com/terms-and-conditions) on Wiley Online Library for rules of use; OA articles are governed by the applicable Creative Commons License

Table 1
Correlation Between Normalized Intensities of Extreme Coastal Events Recorded From 1958 to 2015 Shown in Figure 5, of OLM IEKW Mode 2 (K2; Averaged Within (20°W–0°E, 0°N) and Shifted Forward by One Month (to Lead T10 by One Month, in Agreement With Figure 6)), Coastal T10 and Surface Meridional Wind Stress (TY) Averaged in the Three Coastal Domains (Southern Angola (10°S–15°S), ABF domain (15°S–19°S), and Northern Namibia (19°S–24°S) and Shifted Forward by One Month (in Order to Lead T10 by One Month, in Agreement With Figure 7), Within the 1°-Width Coastal Band)

Correlations	Southern Angola	ABF	Northern Namibia
T10–TY	−0.85	−0.76	−0.42
T10–K2	0.81	0.81	0.83
K2–TY	−0.61	−0.67	−0.5

Note. Correlations are statistically significant at 95%.

anomalies of T10 and TY are slightly greater than the one with IEKW mode 2 in absolute value. However, meridional wind stress is quite weak throughout the year off Angola and the seasonality of the local upwelling there is mainly driven by CTW propagations (Ostrowski et al., 2009; Rouault, 2012). Considering the fact that the Southern Angola domain is more connected than Northern Namibia to the dynamic processes (propagations of IEKW) occurring along the equatorial Atlantic (Imbol Koungue et al., 2017), it is likely that the local link between anomalies of meridional wind stress and T10 in the Southern Angola domain is just the expression of the wind stress variations upstream (see Figure 12). Also, as mentioned in Lübbecke et al. (2010), strong ocean-atmosphere coupling (WES feedback mentioned in section 3.3.2) occurs south of the equator up to ~10°S, east of 20°W over the warming or cooling area. This feedback could contribute to amplify the southerly wind stress along the Angolan coast leading to a high local correlation between anomalies of wind stress and T10. Statistically significant anticorrelations at 95% of −0.61, −0.67, and −0.5 are found between intensities of IEKW mode 2 and TY from Southern Angola to Northern Namibia, respectively (Table 1, third row). It means that one month before the onset of a coastal warm or cold interannual event, downwelling or upwelling IEKW mode 2 propagate along the equatorial Atlantic, whereas weaker or stronger than normal meridional wind stress is present at the southwestern African coast.

Figure 12 depicts the regression coefficients of detrended normalized anomalies of OGCM surface zonal and meridional wind stress (TX, TY) onto DNT10A averaged in Southern Angola (SA), ABF, and Northern

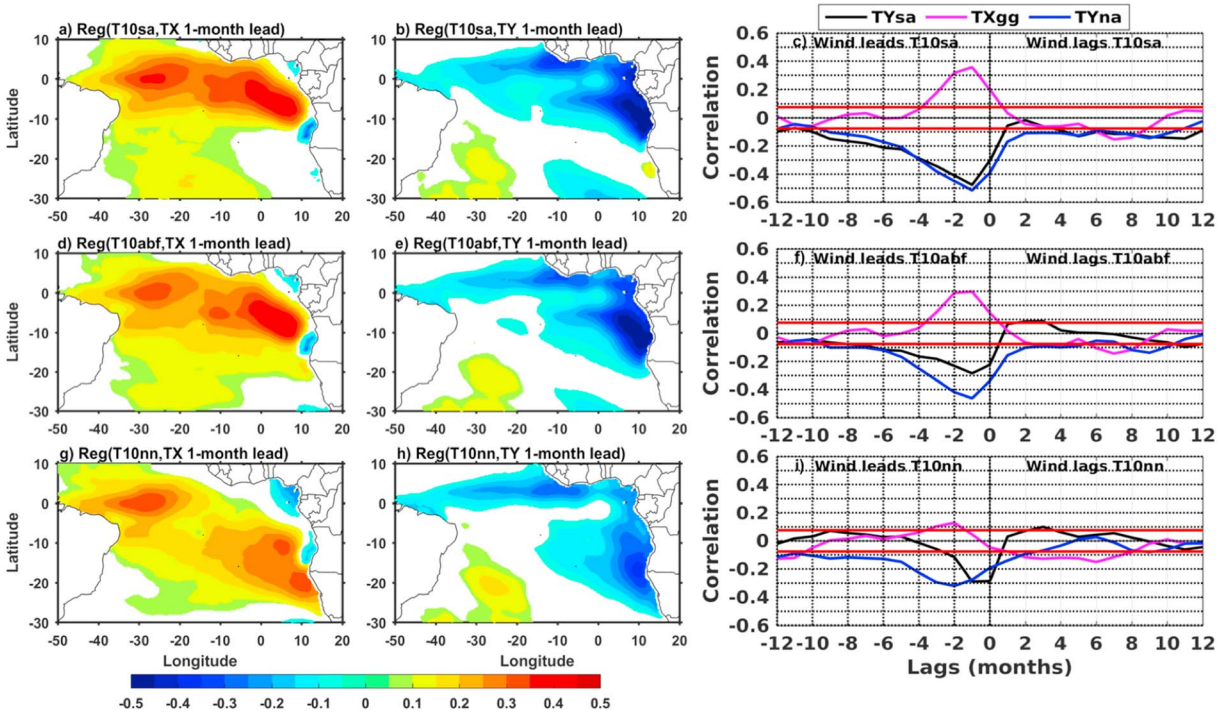

Figure 12. Regression coefficients between detrended normalized anomalies (1958–2015) of (a, d, and g) DFS5.2 surface zonal wind stress (TX) shifted forward by one month onto coastal (averaged within the 1°-width coastal band) OGCM T10 anomalies averaged in Southern Angola (T10sa; 10°S–15°S), ABF domain (T10abf; 15°S–19°S), and Northern Namibia (T10nn; 19°S–24°S), respectively. (b, e, and h) Similar to (a), (d), and (g) but for the regression with OGCM TY. Regression coefficients are statistically significant at 95%. The correlation between monthly detrended normalized anomalies of OGCM T10 averaged in three coastal domains: (c) T10sa, (f) T10abf, and (i) T10nn in function of the lags (in months) and DFS5.2 surface meridional wind stress (TY) averaged locally (in black; same as in Figure 7), DFS5.2 surface zonal wind stress averaged in the Gulf of Guinea (TXgg; averaged within (10°W–4°E, 4°S–7°N), in magenta), and TY averaged in Northern Angola (TYna; from 5°S to 10°S and from the coast to 1° offshore, in blue). Negative lags indicate that surface wind stress leads. Correlations statistically significant at 95% are found outside the correlation thresholds (using *p* value statistical test from Sciremammano (1979)) which are indicated by thick red lines.

21699291, 2019, 8, Downloaded from https://agupubs.onlinelibrary.wiley.com/doi/10.1029/2019JC015013 by Cochrane France, Wiley Online Library on [04/05/2024]. See the Terms and Conditions (https://onlinelibrary.wiley.com/terms-and-conditions) on Wiley Online Library for rules of use; OA articles are governed by the applicable Creative Commons License

21699291, 2019, 8, Downloaded from https://agupubs.onlinelibrary.wiley.com/doi/10.1029/2019JC015013 by Cochrane France, Wiley Online Library on [04/05/2024]. See the Terms and Conditions (https://onlinelibrary.wiley.com/terms-and-conditions) on Wiley Online Library for rules of use; OA articles are governed by the applicable Creative Commons License

Namibia (NN), respectively. Detrended normalized anomalies (using method 1; cf. section 2.3.2) of TX and TY are shifted forward by one month prior to the warming and cooling along the southwestern African coast. Results in Figure 12 highlight areas of the tropical Atlantic Ocean where the DNT10A in the three domains of interest could respond to the wind stress forcing. Similar analysis as in Figure 12 is also performed between the wind stress curl and DNT10A (Figure S1 in the supporting information) to look at the role played by the near-coastal wind stress curl during the onset of the anomalous events.

One month before the onset of the anomalous coastal event, anomalies of T10 in the Southern Angola domain (Figure 12a) seem to be positively (negatively) linked to zonal wind stress fluctuations in two equatorial zones. A positive link means that westerly or easterly zonal wind stress anomalies along the equatorial Atlantic are associated with the occurrence of warming or cooling along in the Southern Angola domain, respectively. The first equatorial region is found around 40°W–20°W from 3°S to 3°N which is an important area where IEKW are forced (Illig et al., 2004; Florenchie et al., 2004; Illig & Dewitte, 2006; Lübbecke et al., 2010; Imbol Koungue et al., 2017) and the second one is east of 20°W in the eastern equatorial Atlantic between 10°W and 10°E from 6°S to 7°N which has been shown to be an area where IEKW are locally forced at interannual (Bachèlery et al., 2016) and subseasonal time scales (Illig et al., 2018). Figure 12b reveals that one month before the onset of the warming (cooling) in the Southern Angola domain, southerly (northerly) wind stress anomalies develop. However, minimum regression coefficient is observed north of 15°S up to the Cameroonian coast extending westward toward the East Brazilian coast with a second minimum along the Sierra Leone coastline.

This confirms that the local meridional wind stress off Angola is part of the large-scale wind stress variations as observed in Figures 10c and 11c. In the Southern Angola domain, results from Figures 12a and 12b show that the form of the Angolan coast favors northeasterly or southwesterly wind stress anomalies to develop which could lead to a local onshore or offshore transport of surface water hence downwelling or upwelling through Ekman dynamics, respectively. This is also confirmed by positive regression coefficient found between T10 and wind stress curl anomalies (Figure S1a in the supporting information). The hypothesis is that positive (negative) DNT10A are associated with weaker (stronger) near-coastal cyclonic wind stress curl relative to the mean situation which in turn would decrease (increase) upwelling-favoring warm (cold) surface temperature anomalies off Southern Angola. Note that the wind stress off Angola is generally weak (Ostrowski et al., 2009), which implies that its contribution to initiate the warming or cooling off Southern Angola could be minor or secondary at the expense of CTW which control the seasonal upwelling off Angola (Ostrowski et al., 2009). Nevertheless, the warm surface temperature anomalies generated by the weak cyclonic wind stress curl could be transported poleward by downwelling CTW. Figure 12c also shows at lag −1 (wind stress leads T10) that detrended normalized anomalies of meridional wind stress in the Northern Angola (in blue) shows a slightly higher correlation (though not significantly higher) with T10 in the Southern Angola domain than the local meridional wind stress (in black) and the zonal wind stress in the Gulf of Guinea (in magenta). These meridional wind stress anomalies in the Northern Angola could generate CTW, which propagate poleward and influence DNT10A in the regions downstream. However, it has been mentioned that IEKW could be locally forced in the Gulf of Guinea (Bachèlery et al., 2016) by zonal wind stress anomalies one month before the onset of the coastal event in the Southern Angola. This IEKW propagates toward the African coast and triggers CTW which would initiate the warming or the cooling in the Southern Angola.

Similarly, Figures 12d and 12e exhibit almost the same patterns of maxima and minima of regression coefficients as Figures 12a and 12b, respectively. This suggests that DNT10A in the ABF domain is more influenced by equatorial forcing (IEKW) or more connected to meridional wind stress anomalies occurring further equatorward. Florenchie et al. (2004) showed that the maximum of SSTA occurs in an area between 10°S and 20°S from 8°E to the African continent called the Angola-Benguela Area. Therefore, both domains (SA and ABF) seem to respond to similar forcing being part of the Angola-Benguela Area. The effect of the position of the coastline off Angola persists and could initiate a downwelling or upwelling in the Southern Angola domain as described in Figure 12a. Figure S1b in the supporting information shows similar patterns of regression coefficients as in Figure S1a in the supporting information. Positive regression coefficients are found between 10°S and 20°S with a maximum in the Southern Angola (>0.4). This highlights the ability of weak (strong) alongshore wind stress to warm (cool) the

surface temperature between 10°S and 20°S. Note that weaker (stronger) alongshore wind stress lead to warming (cooling) via reduced (increased) latent heat flux. Also, weak (strong) cyclonic wind stress curl could lead to a decrease (increase) of the poleward transport across the ABF (Junker et al., 2015).

Results in Figure 12f show that DNT10A in the ABF domain are influenced by CTW triggered in the Northern Namibia one month before the onset of the coastal event.

As observed and described for the two coastal domains upstream, DNT10A in the Northern Namibia domain are linked to CTW triggered by wind forced IEKW in the western equatorial Atlantic (Figure 12g). A second area of strong positive regression coefficients (<0.25) is found off Northern Namibia stretching northwestward and collocated with the minimum regression coefficient area observed in Figure 12h south of ~5°S. This highlights the fact that southeasterly wind stress weakens or strengthen one month prior to the coastal warming or cooling in Northern Namibia. South of 10°S in the southeastern Atlantic Ocean, southeasterly wind stress prevails and is part of the wind stress pattern that forms the SAA. Similar patterns are observed when the wind stress anomalies are taken at lag 0 (not shown). Moreover, positive regression coefficients observed in Figure S1c in the supporting information along the southwestern African coast from 10°S up to ~28°S confirm the weakening (strengthening) of the upwelling-favoring winds prior to the onset of the warming (cooling) of the coastal upwelling of Northern Namibia. Within the upwelling-driven Northern Namibia domain, weak (strong) cyclonic wind stress curl generating negative (positive) Ekman pumping that could decrease (increase) the coastal upwelling resulting in positive (negative) surface temperature anomalies. Lag-correlation analysis (Figure 12i) shows that variations of meridional wind stress in Northern Angola caused anomalies of T10 in Northern Namibia with a lag of two months (correlation of −0.3). This could correspond to the travel time that a CTW triggered in the Northern or Southern Angola takes to reach the Northern Namibia domain and influences the T10. This correlation is equal to the one observed locally (in black) between both variables at lags −1 and 0. The results on the local correlation are described in Figure 7c. However, there is a very low correlation (~0.1) between detrended normalized anomalies of zonal wind stress averaged in Gulf of Guinea and DNT10A in the Northern Namibia at lag −1. Figure 12i suggests that T10 in Northern Namibia could be either under the influence of the local southeasterly wind stress that is part of the SAA or CTW triggered in Northern Angola. Additionally, an important contribution is also coming from IEKW mode 2 triggered in the western equatorial Atlantic (Figure 6c) by a change in the easterly wind stress represented by positive regression coefficients in Figure 12g. The low correlation between anomalies of zonal wind stress in the Gulf of Guinea and T10 in Northern Namibia reveals that CTW emanating from IEKW triggered in the Gulf of Guinea do not seem to play an important role during the onset of the coastal warming or cooling in the Northern Namibia domain. Additionally, meridional transport anomalies across the ABF associated with CTW propagations seem to contribute to the development of the coastal events in Northern Namibia. Positive (weaker poleward flow than seasonal average or equatorward flow) or negative (stronger poleward transport than seasonal average) anomalies of meridional transport across the ABF are associated with negative or positive anomalies of T10 in Northern Namibia, respectively (not shown). A minimum correlation of ~−0.2 statistically significant at 95% is observed when net mass transport anomalies across the ABF lead DT10A in the Northern Namibia domain by two months (not shown).

3.3.4. Summary, Discussion, and Conclusions

The tropical southeastern Atlantic Ocean variability is examined at interannual time scales from 1958 to 2015 with a focus on the variability in the Angola-Benguela upwelling system, along the coast of Angola, Namibian, and South Africa. This study aims at understanding the processes associated with the development of Benguela Niño and Benguela Niña events, their links with the equatorial Atlantic Ocean, and the potential contribution of the local forcing in the southeastern Atlantic Ocean.

In order to investigate the different processes responsible for the onset of anomalous coastal events from 1958 to 2015, a simulation (OGCM) was performed over the tropical Atlantic. The OGCM was then validated using available observation data sets (PIRATA records, satellite, and in situ data). Overall against observed data, the OGCM shows good skills in the southeastern Atlantic Ocean in representing (1) the mean state (temperature and meridional current) including the coastal upwelling feature and (2) the interannual variability of SSH and temperature at 10 m. In addition, the OGCM was skillful in reproducing the dynamical connection between the equatorial domain and the coastal domain (along the southwestern African coast) southward up to ~25°S via the propagation of the IEKW and equatorially forced CTW.

21699291, 2019, 8, Downloaded from https://agupubs.onlinelibrary.wiley.com/doi/10.1029/2019JC015013 by Cochrane France, Wiley Online Library on [04/05/2024]. See the Terms and Conditions (https://onlinelibrary.wiley.com/terms-and-conditions) on Wiley Online Library for rules of use; OA articles are governed by the applicable Creative Commons License

21699291, 2019, 8, Downloaded from https://agupubs.onlinelibrary.wiley.com/doi/10.1029/2019JC015013 by Cochrane France, Wiley Online Library on [04/05/2024]. See the Terms and Conditions (https://onlinelibrary.wiley.com/terms-and-conditions) on Wiley Online Library for rules of use; OA articles are governed by the applicable Creative Commons License

Following the methodology developed in Imbol Koungue et al. (2017), 21 (13 warm and 8 cold) extreme coastal events are selected over the period 1958 to 2015. Three newly identified warm interannual coastal events are documented, namely, the extreme warm events 1958/1959 (December–July), 1960/1961 (September–April), and 1974 (April–July). Similarly, undocumented extreme cold events are identified in 1965 (September–December), 1980/1981 (October–April), and 1985 (March–June). Five out of 21 of these new extreme events occur before the satellite era (before 1982). Note that little differences are observed in the timing of the events (start and end) compared to the identified events in the recent study by Imbol Koungue et al. (2017) carried out over the PIRATA period from 1998 to 2012. For example, Imbol Koungue et al. (2017) and Rouault et al. (2018) identified the 2010/2011 extreme warm event between November and April while it is recorded between September 2010 and April 2011 using the OGCM over 1958 to 2015. Difference in timing of the event can be attributed to the difference in length of the time series which yields different monthly climatology, standard deviations, and then different normalized anomalies and thresholds. Also, the fact that the OGCM does not perfectly agree with observations and the presence of warm bias in the Angola-Benguela upwelling system (Figure 2b at 23°S) could impact the time series by increasing or reducing the duration of a coastal event. This could also justify the fact that some anomalous coastal events identified by Imbol Koungue et al. (2017) are missing in this study, for instance, coastal warm events 2003 (July–December) and 2008/2009 (November–January) which do not fulfill the criterion over the 1958–2015 period. Another source of discrepancies between coastal events duration or intensities of simulated and observed events is the fact that the interannual variability of river runoff is not taken into account in the OGCM. For instance, Lübbecke et al. (2019) recently suggested that the interannual variability of precipitation over Southern Africa leading to a freshwater anomaly off Angola via runoff of Congo and possibly other small rivers could have played a role in forcing the 2016 warm event.

FMA averages (Figures 4 and 8) of all the extreme coastal events show warming or cooling pattern along the southwestern African coast. The strongest warming occurs in FMA 1963 (1962/1963 event) and the strongest cooling in FMA 1997 (1996/1997 event). Over the 1958 to 2015 period, most of the anomalous coastal warm or cold events including the newly identified ones are linked to downwelling or upwelling IEKW mode 2 propagations in agreement with previous studies (Imbol Koungue et al., 2017). There is a one-month lag when detrended anomalies of IEKW mode 2 lead surface temperature anomalies in Southern Angola and the ABF domain. This finding agrees with the recent study of Imbol Koungue et al. (2017).

In the tropical Atlantic Ocean, extreme coastal events that peak in March–April show a warming or cooling pattern that is observed up to ~25°S along the Namibian coastline. This latitude corresponds to the southernmost latitude where the CTW propagations can be detected on the surface temperature signal anomalous coastal events. This is consistent with the work of Bachèlery et al. (2016). We observe an asymmetry of Benguela Niño/Niña events. First, Benguela Niña events last longer than Benguela Niño events which agree with the finding of Florenchie et al. (2004). Second, we have observed that the spatial area of cold DT10A during a Benguela Niña event is broader than the one of warm DT10A during a Benguela Niño, occasionally covering the whole south Atlantic (Figures 8d and 11d). Third, the WES feedback seems to be more active during a Benguela Niño than a Benguela Niña from Figures 10c and 11c. More analyses are necessary to investigate the role of this feedback in more details. Lastly, the meridional dipole observed on the Benguela Niño composite maps is not observed on the Benguela Niña composite maps. This means that March-April Benguela Niña events appear to be independent of other air-sea interactions in the tropical North Atlantic. A tendency of Atlantic Niño to follow Benguela Niño with a lag of about two months is observed, which is consistent with the previous findings (Lübbecke et al., 2010; Richter et al., 2010; Rouault et al., 2009). Both forcings (local and remote) are found as part of basin-scale weakening or strengthening of the SAA and associated wind stress during Benguela Niño or Niña, respectively. This is consistent with the 1958–2000 modeling study of Lübbecke et al. (2010) in which correlation map between April SST and February wind stress revealed that the whole SAA partly formed of weak trade winds along the equator and weak coastal winds, weakened prior to the warming in the BUS.

We suggest that the WES feedback is at work one month before the peak and during the peak of the event, as northwesterly or southeasterly wind stress anomalies are present over the warming or cooling area south of the equator, respectively (Figures 10c, 10d, 11c, and 11d). Similar assumptions have been made in the study of Lübbecke et al. (2010) for the tropical Atlantic. Moreover, there could be a possibility that the ocean-

21699291, 2019, 8, Downloaded from https://agupubs.onlinelibrary.wiley.com/doi/10.1029/2019JC015013 by Cochrane France, Wiley Online Library on [04/05/2024]. See the Terms and Conditions (https://onlinelibrary.wiley.com/terms-and-conditions) on Wiley Online Library for rules of use; OA articles are governed by the applicable Creative Commons License

atmosphere coupling has impacted the local alongshore wind stress off Angola by weakening or strengthening them before the peak of the warm or cold coastal events, respectively, in Southern Angola. This could partly explain the high anticorrelation (~−0.5) between anomalies of T10 and meridional wind stress in Southern Angola compared to the other domains (Figure 7a and Table 1). However, there is a total absence of upwelling-favoring winds in Southern Angola (Ostrowski et al., 2009; Rouault, 2012). We have shown that the equatorial wind forcing resulting from the variations of zonal wind stress in the western/central (Illig et al., 2004; Florenchie et al., 2004; Lübbecke et al., 2010; Bachèlery et al., 2016; Imbol Koungue et al., 2017) and eastern equatorial Atlantic (Gulf of Guinea; Bachèlery et al., 2016) trigger IEKW which at the African coast initiate poleward propagating CTW which influence T10 along the southwestern African coast. We suggest that variations of meridional wind stress north of 15°S mainly in the Northern Angola domain (5°S–10°S, from the coast to 1° offshore) could also trigger local CTW which clearly influence T10 from Southern Angola to Northern Namibia (Figures 12c, 12f, and 12i). On top of that, weak (strong) cyclonic wind stress curl observed near the coast off Southern Angola could generate warm (cold) surface temperature anomalies by decreasing (increasing) the near-coastal upwelling. Weaker (stronger) wind could also lead to a warming (cooling) by reducing (enhancing) the turbulent latent heat flux at the sea surface (Lübbecke et al., 2019). Across the ABF, the poleward transport could be weakened by weak cyclonic wind stress curl (Junker et al., 2015) and surface temperature anomalies will be propagated poleward by downwelling CTW. At interannual time scales, meridional transport anomalies across the ABF might then contribute to the development of anomalous coastal events in Northern Namibia. A lag of one to two months (not shown) is found when detrended anomalies of net mass transport across the ABF lead surface temperature anomalies in the Northern Namibia domain which is consistent with the study of Rouault (2012), who reported a lag ranging between two and four months. The fact that maximum anticorrelation occurs at two-month lag (one month before the IEKW mode 2 forcing) could be due to the contribution of higher-order IEKW modes which propagate slower than IEKW mode 2 or to the effect of the large-scale wind stress forcing. Therefore, the advection of anomalous warm or cold waters across the ABF and its link to anomalous coastal events in Northern Namibia can be partly explained by the net mass transport across the ABF. We have shown that T10 in Northern Namibia is less influenced by equatorial dynamics compared to the two other domains further upstream (Rouault, 2012). Similar wind stress forcings as in the two other domains are observed except the zonal wind stress in the Gulf of Guinea which is weak. Due to the upwelling dynamics in Northern Namibia associated with a low local stratification depending on the season (Imbol Koungue et al., 2017), the imprint of CTW on at the ocean surface is not well observed. This could also justify the low correlation compared to other domains statistically significant at 95% observed between different parameters and DNT10A (Figures 6c, 12c, 12f, and 12i). Furthermore, we have shown that DNT10A are also impacted by local alongshore wind stress which is part of SAA. The recent study from Rouault et al. (2018) showed that during the onset of the 2010/2011 Benguela Niño, the southeasterly wind stress (upwelling-favoring wind) weakened off Namibia due to the equatorward shift of the SAA leading to above normal SST. They further claimed that these large-scale movements in the SAA involving wind stress in the tropical and South Atlantic are at the origin of many Benguela Niño and Atlantic Niño events as also proposed by Lübbecke et al. (2010, 2014). Weak (strong) local cyclonic wind stress curl observed near the Namibian coastline generate negative (positive) Ekman pumping and decrease (increase) the near-coastal upwelling leading to the apparition of positive (negative) surface temperature anomalies. A potential contribution of the local surface heat fluxes during the onset of the anomalous coastal events has not been thoroughly investigated in this study but is briefly discussed. Past studies (Bachèlery et al., 2016; Florenchie et al., 2004; Rouault et al., 2007) showed that local surface heat fluxes tend to damp the anomalous coastal events in the Angola-Benguela Area box, but they could also modulate their origin (Lübbecke et al., 2019).

In conclusion, an OLM can be a useful tool to investigate the IEKW propagations along the equatorial Atlantic which are linked to Benguela Niños or Niñas in the Angola-Benguela upwelling system as it was the case for the newly identified extreme coastal events that developed before 1982. The importance of the implementation of an early warning system using OLM forced with real-time satellite wind estimates or atmospheric model outputs in combination with real-time PIRATA buoy records and altimetry has already been mentioned in the recent study by Imbol Koungue et al. (2017). Tide gauge and current meter available in real time in Angola and Namibia would complete the system and are much needed. During the peak season of Benguela Niño and Niña (March–April), warming or cooling pattern is observed up to ~25°S along the

21699291, 2019, 8, Downloaded from https://agupubs.onlinelibrary.wiley.com/doi/10.1029/2019JC015013 by Cochrane France, Wiley Online Library on [04/05/2024]. See the Terms and Conditions (https://onlinelibrary.wiley.com/terms-and-conditions) on Wiley Online Library for rules of use; OA articles are governed by the applicable Creative Commons License

Namibian coastline. A tendency of Atlantic Niño or Niña to follow Benguela Niño or Niña has been observed, and a possible asymmetry of Benguela Niño/Niña was suggested in this study. Local and remote forcing which are part of basin-scale weakening or strengthening of the wind stress one to two months before the peak of Benguela Niño or Niña have been evidenced. Ocean-atmosphere coupling seems to be at work as northwesterly or southeasterly wind stress anomalies are observed over the warming or cooling area south of the equator east of 20°W. DT10A in Southern Angola and ABF domains have shown to be influenced by equatorial dynamics (CTW emanating from IEKW) via variations of zonal wind stress in the western and eastern equatorial Atlantic and CTW forced in the Northern/Southern Angola by meridional wind stress anomalies part of the large-scale wind stress forcing. However, DT10A in Northern Namibia is impacted by local southeasterly wind stress anomalies part of the SAA and CTW triggered by IEKW forced by variations of zonal wind stress anomalies in the western equatorial Atlantic and CTW forced by meridional wind stress anomalies in the Southern/Northern Angola. Across the ABF, the interaction between CTW and local currents leads to the advection of warm or cold waters into the Northern Benguela upwelling system which is a key factor for the development of anomalous coastal events.

Further work will involve a study of the role of local variability (strength of local stratification, cloud cover, Ekman transport, and turbulent fluxes) for each Benguela Niño and Benguela Niña event over 1958–2015. A high-resolution coupled ocean-atmosphere model could help to analyze the role of the local coupled feedback (WES feedback) in more details. Also, the role of the near coastal wind stress curl which drives the poleward boundary current needs to be better ascertained during the onset of these anomalous coastal events.

Acknowledgments
The authors want to acknowledge ACCESS, NRF, DST, WRC, LMI ICEMASA, the SARCHI chair of Ocean Atmosphere Modelling, and the Nansen Tutu for Marine Environmental Research for funding. The research leading to these results received funding from the EU FP7/2007–2013 under grant agreement 603521 PREFACE project and from the EU H2020 under grant agreement 817578 TRIATLAS project. It was further supported by the German Federal Ministry of Education and Research as part of the SACUS II (03F0751A), BANINO (03F0795A) and RACE (03F0824C) projects. Model outputs used in this study are freely available at https://doi.org/10.6084/m9.figshare.8224394.v1.

References

Bachèlery, M. L., Illig, S., & Dadou, I. (2016). Interannual variability in the South-East Atlantic Ocean, focusing on the Benguela Upwelling System: Remote versus local forcing. *Journal of Geophysical Research: Oceans*, *121*, 284–310. https://doi.org/10.1002/2015JC011168

Bakun, A., & Nelson, C. S. (1991). The seasonal cycle of wind stress curl in subtropical eastern boundary current regions. *Journal of Physical Oceanography*, *21*, 1815–1834.

Binet, D., Gobert, B., & Maloueki, L. (2001). El Niño-like warm events in the Eastern Atlantic (6°N, 20°S) and fish availability from Congo to Angola (1964–1999). *Aquatic Living Resources*, *14*, 99–113.

Blamey, L. K., Shannon, L. J., Bolton, J. J., Crawford, R. J. M., Dufois, F., EversKing, H., et al. (2015). Ecosystem change in the southern Benguela and the underlying processes. *Journal of Marine Systems*, *144*, 9–29. https://doi.org/10.1016/j.jmarsys.2014.11.006

Bourlès, B., Lumpkin, R., McPhaden, M. J., Hernandez, F., Nobre, P., Campos, E., et al. (2008). The PIRATA program: History, accomplishments, and future directions. *Bulletin of the American Meteorological Society*, *89*(8), 1111–1126. https://doi.org/10.1175/2008BAMS2462.1

Boyer, D. C., Boyer, H. J., Fossen, I., & Kreiner, A. (2001). Changes in abundance of the northern Benguela sardine stock during the decade 1990–2000, with comments on the relative importance of fishing and the environment. *African Journal of Marine Science*, *23*(1), 67–84. https://doi.org/10.2989/025776101784528854

Chavez, F. P., & Messié, M. (2009). A comparison of eastern boundary upwelling ecosystems. *Progress in Oceanography*, *83*(1–4), 80–96. https://doi.org/10.1016/j.pocean.2009.07.032

Clarke, A. J. (1983). The reflection of equatorial waves from oceanic boundaries. *Journal of Physical Oceanography*, *13*(7), 1193–1207. https://doi.org/10.1175/1520-0485(1983)013<1193:TROEWF>2.0.CO;2

Colberg, F., & Reason, C. J. C. (2006). A model study of the Angola Benguela Frontal Zone: Sensitivity to atmospheric forcing. *Geophysical Research Letters*, *33*, L19608. https://doi.org/10.1029/2006GL027463

Dai, A., & Trenberth, K. E. (2002). Estimates of freshwater discharge from continents: Latitudinal and seasonal variations. *Journal of Hydrometeorology*, *3*(6), 660–687. https://doi.org/10.1175/1525-7541(2002)003<0660:EOFDFC>2.0.CO;2

Dee, D. P., Uppala, S. M., Simmons, A. J., Berrisford, P., Poli, P., Kobayashi, S., et al. (2011). The ERA-Interim reanalysis: Configuration and performance of the data assimilation system. *Quarterly Journal of the Royal Meteorological Society*, *137*(656), 553–597.

Diaconis, P., & Efron, B. (1983). Computer-intensive methods in statistics. *Scientific American*, *248*(5), 116–130. https://doi.org/10.1038/scientificamerican0583-116

Ducet, N., Le Traon, P. Y., & Reverdin, G. (2000). Global high-resolution mapping of ocean circulation from TOPEX/Poseidon and ERS-1 and-2. *Journal of Geophysical Research*, *105*(C8), 19,477–19,498. https://doi.org/10.1029/2000JC900063

Dussin, R., Barnier, B., & Brodeau, L. (2016). The making of Drakkar forcing set DFS5, DRAKKAR/MyOcean Rep. 01–04-16, Laboratoire de Glaciologie et Géophysique de l'Environnement, Grenoble, France.

Efron, B. (1977). Bootstrap methods: Another look at the jackknife. *Annals of Statistics*, *7*, 1–26.

Fennel, W., Junker, T., Schmidt, M., & Mohrholz, V. (2012). Response of the Benguela upwelling systems to spatial variations in the wind stress. *Continental Shelf Research*, *45*, 65–77. https://doi.org/10.1016/j.csr.2012.06.004

Florenchie, P., Lutjeharms, J. R., Reason, C. J. C., Masson, S., & Rouault, M. (2003). The source of Benguela Niños in the South Atlantic Ocean. *Geophysical Research Letters*, *30*(10), 1505. https://doi.org/10.1029/2003GL017172

Florenchie, P., Reason, C. J. C., Lutjeharms, J. R. E., Rouault, M., Roy, C., & Masson, S. (2004). Evolution of interannual warm and cold events in the southeast Atlantic Ocean. *Journal of Climate*, *17*(12), 2318–2334. https://doi.org/10.1175/1520-0442(2004)017<2318:EOIWAC>2.0.CO;2

Gammelsrød, T., Bartholomae, C. H., Boyer, D. C., Filipe, V. L. L., & O'Toole, M. J. (1998). Intrusion of warm surface water along the Angolan-Namibian coast in February–March 1995: The 1995 Benguela Niño. *South African Journal of Marine Science*, *19*(1), 41–56. https://doi.org/10.2989/025776198784126719

Grotjahn, R., & Faure, G. (2008). Composite predictor maps of extraordinary weather events in the Sacramento, California, region. *Weather and Forecasting*, *23*(3), 313–335. https://doi.org/10.1175/2007WAF2006055.1

Hansingo, K., & Reason, C. J. C. (2009). Modelling the atmospheric response over southern Africa to SST forcing in the southeast tropical Atlantic and southwest subtropical Indian Oceans. *International Journal of Climatology*, *29*(7), 1001–1012. https://doi.org/10.1002/joc.1919

Hardman-Mountford, N. J., Richardson, A. J., Agenbag, J. J., Hagen, E., Nykjaer, L., Shillington, F. A., & Villacastin, C. (2003). Ocean climate of the south east Atlantic observed from satellite data and wind models. *Progress in Oceanography*, *59*(2-3), 181–221. https://doi.org/10.1016/j.pocean.2003.10.001

Hernandez, O., Jouanno, J., & Durand, F. (2016). Do the Amazon and Orinoco freshwater plumes really matter for hurricane-induced ocean surface cooling? *Journal of Geophysical Research: Oceans*, *121*, 2119–2141. https://doi.org/10.1002/2015JC011021

Hernandez, O., Jouanno, J., Echevin, V., & Aumont, O. (2017). Modification of sea surface temperature by chlorophyll concentration in the Atlantic upwelling systems. *Journal of Geophysical Research: Oceans*, *122*, 5367–5389. https://doi.org/10.1002/2016JC012330

Hisard, P., Hénin, C., Houghton, R., Piton, B., & Rual, P. (1986). Oceanic conditions in the tropical Atlantic during 1983 and 1984. *Nature*, *322*(6076), 243–245. https://doi.org/10.1038/322243a0

Hormann, V., & Brandt, P. (2009). Upper equatorial Atlantic variability during 2002 and 2005 associated with equatorial Kelvin waves. *Journal of Geophysical Research*, *114*, C03007. https://doi.org/10.1029/2008JC005101

Hu, Z. Z., & Huang, B. (2007). Physical processes associated with the tropical Atlantic SST gradient during the anomalous evolution in the southeastern ocean. *Journal of Climate*, *20*(14), 3366–3378. https://doi.org/10.1175/JCLI4189.1

Illig, S., & Bachèlery, M. L. (2019). Propagation of subseasonal equatorially-forced coastal trapped waves down to the Benguela upwelling system. *Scientific Reports*, *9*(1), 5306. https://doi.org/10.1038/s41598-019-41847-1

Illig, S., Bachèlery, M. L., & Cadier, E. (2018). Subseasonal coastal-trapped wave propagations in the southeastern Pacific and Atlantic Oceans: 2. Wave characteristics and connection with the equatorial variability. *Journal of Geophysical Research: Oceans*, *123*, 3942–3961. https://doi.org/10.1029/2017JC013540

Illig, S., & Dewitte, B. (2006). Local coupled equatorial variability versus remote ENSO forcing in an intermediate coupled model of the tropical Atlantic. *Journal of Climate*, *19*(20), 5227–5252. https://doi.org/10.1175/JCLI3922.1

Illig, S., Dewitte, B., Ayoub, N., Du Penhoat, Y., Reverdin, G., De Mey, P., et al. (2004). Interannual long equatorial waves in the tropical Atlantic from a high-resolution ocean general circulation model experiment in 1981–2000. *Journal of Geophysical Research*, *109*, C02022. https://doi.org/10.1029/2003JC001771

Jouanno, J., Hernandez, O., & Sanchez-Gomez, E. (2017). Equatorial Atlantic interannual variability and its relation to dynamic and thermodynamic processes. *Earth System Dynamics*, *8*(4), 1061–1069. https://doi.org/10.5194/esd-8-1061-2017

Jouanno, J., Marin, F., Du Penhoat, Y., Sheinbaum, J., & Molines, J. M. (2011). Seasonal heat balance in the upper 100 m of the equatorial Atlantic Ocean. *Journal of Geophysical Research*, *116*, C09003. https://doi.org/10.1029/2010JC006912

Junker, T., Mohrholz, V., Siegfried, L., & van der Plas, A. (2017). Seasonal to interannual variability of water mass characteristics and currents on the Namibian shelf. *Journal of Marine Systems*, *165*, 36–46. https://doi.org/10.1016/j.jmarsys.2016.09.003

Junker, T., Schmidt, M., & Mohrholz, V. (2015). The relation of wind stress curl and meridional transport in the Benguela upwelling system. *Journal of Marine Systems*, *143*, 1–6. https://doi.org/10.1016/j.jmarsys.2014.10.006

Katz, E. J. (1977). Zonal pressure-gradient along equatorial Atlantic. *Journal of Marine Research*, *35*(2), 293–307.

Kopte, R., Brandt, P., Dengler, M., Tchipalanga, P. C. M., Macuéria, M., & Ostrowski, M. (2017). The Angola Current: Flow and hydrographic characteristics as observed at 11°S. *Journal of Geophysical Research: Oceans*, *122*, 1177–1189. https://doi.org/10.1002/2016JC012374

Imbol Koungue, R. A., Illig, S., & Rouault, M. (2017). Role of interannual Kelvin wave propagations in the equatorial Atlantic on the Angola Benguela Current system. *Journal of Geophysical Research: Oceans*, *122*, 4685–4703. https://doi.org/10.1002/2016JC012463

Large, W. G., & Yeager, S. G. (2009). The global climatology of an interannually varying air–sea flux dataset. *Climate Dynamics*, *33*(2-3), 341–364. https://doi.org/10.1007/s00382-008-0441-3

Le Traon, P. Y., Nadal, F., & Ducet, N. (1998). An improved mapping method of multisatellite altimeter data. *Journal of Atmospheric and Oceanic Technology*, *15*(2), 522–534. https://doi.org/10.1175/1520-0426

Locarnini, R. A., Mishonov, A. V., Antonov, J. I., Boyer, T. P., Garcia, H. E., Baranova, O. K., et al. (2013). World Ocean Atlas 2013, Volume 1: Temperature. S. Levitus, Ed., A. Mishonov Technical Ed.; NOAA Atlas NESDIS 73, 40 pp.

Lübbecke, J., Brandt, P., Dengler, M., Kopte, R., Lüdke, J., Richter, I., et al. (2019). Causes and evolution of the southeastern tropical Atlantic warm event in early 2016. *Climate Dynamics*, *53*(1-2), 261–274. https://doi.org/10.1007/s00382-018-4582-8

Lübbecke, J. F., Böning, C. W., Keenlyside, N. S., & Xie, S.-P. (2010). On the connection between Benguela and equatorial Atlantic Niños and the role of the South Atlantic Anticyclone. *Journal of Geophysical Research*, *115*, C09015. https://doi.org/10.1029/2009JC005964

Lübbecke, J. F., Burls, N. J., Reason, C. J. C., & McPhaden, M. J. (2014). Variability in the South Atlantic Anticyclone and the Atlantic Niño Mode. *Journal of Climate*, *27*(21), 8135–8150. https://doi.org/10.1175/JCLI-D-14-00202.1

Lutz, K., Rathmann, J., & Jacobeit, J. (2013). Classification of warm and cold water events in the eastern tropical Atlantic Ocean. *Atmospheric Science Letters*, *14*(2), 102–106. https://doi.org/10.1002/asl2.424

Madec, G. (2014). NEMO ocean engine (Draft edition r5171). Note du Pôle de modélisation, No. 27, Inst. Pierre-Simon Laplace, France, 1288–1619.

Maraldi, C., Chanut, J., Levier, B., Ayoub, N., De Mey, P., Reffray, G., et al., and Mercator Team. (2013). NEMO on the shelf: Assessment of the Iberia-Biscay-Ireland configuration. *Ocean Science*, *9*, 745–771, 4, https://doi.org/10.5194/os-9-745-2013

Maritorena, S., Hembise Fanton d'Andon, O., Mangin, A., Siegel, D., & A. (2010). Merged satellite ocean color data products using a bio-optical model: Characteristics, benefits and issues. *Remote Sensing of Environment*, *114*(8), 1791–1804. https://doi.org/10.1016/j.rse.2010.04.002

Merle, J. (1980). Variabilité thermique annuelle et interannuelle de l'océan Atlantique équatorial est. L'hypothèse d'un El Niño Atlantique. *Oceanologica Acta*, *3*, 209–220.

Mohrholz, V., Schmidt, M., Lutjeharms, J., & R., E. (2001). The hydrography and dynamics of the Angola–Benguela frontal zone and environment in April 1999, South Afr. *Journal of Scientific*, *97*, 199–208.

Morel, A., Berthon, J., & F. (1989). Surface pigments, algal biomass profiles, and potential production of the euphotic layer: Relationships reinvestigated in view of remote-sensing applications. *Limnology and Oceanography*, *34*(8), 1545–1562. https://doi.org/10.4319/lo.1989.34.8.1545

21699291, 2019, 8, Downloaded from https://agupubs.onlinelibrary.wiley.com/doi/10.1029/2019JC015013 by Cochrane France, Wiley Online Library on [04/05/2024]. See the Terms and Conditions (https://onlinelibrary.wiley.com/terms-and-conditions) on Wiley Online Library for rules of use; OA articles are governed by the applicable Creative Commons License

Okumura, Y., & Xie, S. P. (2004). Interaction of the Atlantic equatorial cold tongue and the African monsoon. *Journal of Climate*, *17*(18), 3589–3602. https://doi.org/10.1175/1520-0442(2004)017<3589:IOTAEC>2.0.CO;2

Ostrowski, M., Da Silva, J. C., & Bazik-Sangolay, B. (2009). The response of sound scatterers to El Niño-and La Niña-like oceanographic regimes in the southeastern Atlantic. *ICES Journal of Marine Science*, *66*(6), 1063–1072. https://doi.org/10.1093/icesjms/fsp102

Polo, I., Rodriguez-Fonseca, B., Losada, T., & Garcia-Serrano, J. (2008). Tropical Atlantic variability modes (1979–2002). Part I: Time-evolving SST modes related to West African rainfall. *Journal of Climate*, *21*(24), 6457–6475. https://doi.org/10.1175/2008JCI2607.1

Rayner, N. A., Parker, D. E., Horton, E. B., Folland, C. K., Alexander, L. V., Rowell, D. P., et al. (2003). Global analyses of sea surface temperature, sea ice, and night marine air temperature since the late nineteenth century. *Journal of Geophysical Research*, *108*(D14), 4407. https://doi.org/10.1029/2002JD002670

Reason, C. J. C., Florenchie, P., Rouault, M., & Veitch, J. (2006). 10 Influences of large scale climate modes and Agulhas system variability on the BCLME region. In *Large Marine Ecosystems*, (Vol. 14, pp. 223–238). Elsevier.

Reffray, G., Bourdalle-Badie, R., & Calone, C. (2015). Modelling turbulent vertical mixing sensitivity using a 1-D version of NEMO. *Geoscientific Model Descriptions*, *8*(1), 69–86. https://doi.org/10.5194/gmd-8-69-2015

Reynolds, R. W., Rayner, N. A., Smith, T. M., Stokes, D. C., & Wang, W. (2002). An improved in situ and satellite SST analysis for climate. *Journal of Climate*, *15*, 1609–1625. https://doi.org/10.1175/1520-0442(2002)015<1609:AIISAS>2.0.CO;2

Richter, I., Behera, S. K., Masumoto, Y., Taguchi, B., Komori, N., & Yamagata, T. (2010). On the triggering of Benguela Niños: Remote equatorial versus local influences. *Geophysical Research Letters*, *37*, L20604. https://doi.org/10.1029/2010GL0444461

Rouault, M. (2012). Bi-annual intrusion of tropical water in the northern Benguela upwelling. *Geophysical Research Letters*, *39*, L12606. https://doi.org/10.1029/2012GL052099

Rouault, M., Florenchie, P., Fauchereau, N., & Reason, C. J. C. (2003). South East tropical Atlantic warm events and southern African rainfall. *Geophysical Research Letters*, *30*(5), 8009. https://doi.org/10.1029/2003GL014840

Rouault, M., Illig, S., Bartholomae, C., Reason, C. J. C., & Bentamy, A. (2007). Propagation and origin of warm anomalies in the Angola Benguela upwelling system in 2001. *Journal of Marine Systems*, *68*(3-4), 473–488. https://doi.org/10.1016/j.jmarsys.2006.11.010

Rouault, M., Illig, S., Lübbecke, J., Imbol, K., & R., A. (2018). Origin, development and demise of the 2010–2011 Benguela Niño. *Journal of Marine Systems*, *188*, 39–48. https://doi.org/10.1016/j.jmarsys.2017.07.007

Rouault, M., Servain, J., Reason, C. J. C., Bourlès, B., Rouault, M. J., & Fauchereau, N. (2009). Extension of PIRATA in the tropical South-East Atlantic: An initial one-year experiment. *African Journal of Marine Science*, *31*(1), 63–71. https://doi.org/10.2989/AJMS.2009.31.1.5.776

Sciremammano, F. (1979). A suggestion for the presentation of correlations and their significance levels. *Journal of Physical Oceanography*, *9*(6), 1273–1276. https://doi.org/10.1175/1520-0485(1979)009<1273:ASFTPO>2.0.CO;2

Servain, J., Busalacchi, A. J., McPhaden, M. J., Moura, A. D., Reverdin, G., Vianna, M., & Zebiak, S. E. (1998). A pilot research moored array in the tropical Atlantic (PIRATA). *Bulletin of the American Meteorological Society*, *79*(10), 2019–2031. https://doi.org/10.1175/1520-0477(1998)079<2019:APRMAI>2.0.CO;2

Shannon, L. V. (1985). The Benguela ecosystem, Part I. Evolution of the Benguela, physical features and processes. *Oceanography and Marine Biology: An Annual Review*, *23*, 105–182.

Shannon, L. V., Agenbag, J. J., & Buys, M. E. L. (1987). Large- and mesoscale features of the Angola-Benguela front. *South African Journal of Marine Science*, *5*(1), 11–34. https://doi.org/10.2989/025776187784522261

Shannon, L. V., Boyd, A. J., Brundrit, G. B., & Taunton-Clark, J. (1986). On the existence of an El Niño-type phenomenon in the Benguela system. *Journal of Marine Research*, *44*(3), 495–520. https://doi.org/10.1357/002224086788403105

Stander, G. H., & De Decker, A. H. B. (1969). Some physical and biological aspects of an oceanographic anomaly off South West Africa in 1963. Investigational Report 81, Division of Sea Fisheries, South Africa, 46 pp.

Taylor, K. E. (2001). Summarizing multiple aspects of model performance in a single diagram. *Journal of Geophysical Research*, *106*(D7), 7183–7192. https://doi.org/10.1029/2000JD900719

Tchipalanga, P., Dengler, M., Brandt, P., Kopte, R., Macuéria, M., Coelho, P., et al. (2018). Eastern boundary circulation and hydrography off Angola–building Angolan oceanographic capacities. *Bulletin of the American Meteorological Society*, *99*(8), 1589–1605. https://doi.org/10.1175/BAMS-D-17-0197.1

Umlauf, L., & Burchard, H. (2003). A generic length-scale equation for geophysical turbulence models. *Journal of Marine Research*, *61*(2), 235–265. https://doi.org/10.1357/002224003322005087

Veitch, J. A., Florenchie, P., & Shillington, F. A. (2006). Seasonal and interannual fluctuations of the Angola–Benguela Frontal Zone (ABFZ) using 4.5 km resolution satellite imagery from 1982 to 1999. *International Journal of Remote Sensing*, *27*(5), 987–998. https://doi.org/10.1080/01431160500127914

Walker, N. D. (1987). Interannual sea surface temperature variability and associated atmospheric forcing within the Benguela system. *South African Journal of Marine Science*, *5*(1), 121–132. https://doi.org/10.2989/025776187784522108

21699291, 2019, 8, Downloaded from https://agupubs.onlinelibrary.wiley.com/doi/10.1029/2019JC015013 by Cochrane France, Wiley Online Library on [04/05/2024]. See the Terms and Conditions (https://onlinelibrary.wiley.com/terms-and-conditions) on Wiley Online Library for rules of use; OA articles are governed by the applicable Creative Commons License